Finite Element Analysis of UOE Manufacturing Process and its Effect on Mechanical Behavior of Offshore Pipes

FINITE ELEMENT ANALYSIS OF UOE MANUFACTURING PROCESS AND ITS EFFECT ON MECHANICAL BEHAVIOR OF OFFSHORE PIPES

Giannoula Chatzopoulou, Spyros A. Karamanos[1]

Department of Mechanical Engineering
University of Thessaly, Volos, Greece

George E. Varelis [2]

PDL Solutions (Europe) Ltd
Hexham, United Kingdom

ABSTRACT

Thick-walled steel pipes during their installation in deep-water are subjected to a combination of loading in terms of external pressure, bending and axial tension, which may trigger structural instability due to excessive pipe ovalization. The resistance of offshore pipes against this instability depends on imperfections and residual stresses due to the line pipe manufacturing process. The present study examines the effect of UOE line pipe manufacturing process on the structural response and resistance of offshore pipes during the installation process using advanced finite element simulation tools. The cold bending induced by the UOE process is simulated rigorously and, subsequently, the application of external pressure and structural loading (bending or axial force) is modeled, until structural instability is reached. A parametric analysis is conducted, focusing on the effects of line pipe expansion on the structural capacity of the pipe. The results show that there exists an optimum expansion at which the highest pressure capacity is achieved. The effect of the axial tension on the pressure capacity of the pipe is examined as well. The influence of the line pipe expansion on bending capacity in the presence of external pressure is also identified. Finally, a simplified methodology is employed, accounting for the material anisotropy induced by the manufacturing process, capable of determining the structural capacity of a UOE pipe in a simple and efficient manner with good accuracy, using more conventional modeling tools.

1 INTRODUCTION

Current design philosophy for the mechanical design of deep offshore pipelines is based on the limit-state design approach [1], which considers all possible limit states

1 corresponding author. Tel.+30 24210 74086, FAX. +30 24210 74012, email: skara@mie.uth.gr
2 formerly at Dept. of Mechanical Engineering, University of Thessaly, Volos, Greece

that represent pipeline failure modes, especially during deep-water installation procedure. Pipe resistance under external pressure is the dominant design parameter, and the corresponding failure mode, referred to as “collapse”, is associated with cross-sectional ovalization [1]. To resist high external pressure, deep offshore steel pipes are quite thick, with diameter-to-thickness ratio (D/t) less than 25, and buckle in the inelastic range. Previous work has shown that the initial ovality of pipe cross-section, the anisotropy of pipe steel material, as well as the presence of residual stresses may have significant influence on external pressure capacity [2][3]. Furthermore, during deep water pipeline installation, tension influences pressure capacity at the suspended parts of the pipeline [3][4].

Longitudinal bending of the pipeline in the presence of external pressure, mainly during the installation process, may also lead to structural instability in the form of a limit moment due to ovalization [5][6]. For the thick-walled steel pipes under consideration, this limit (maximum) moment occurs before pipe wall wrinkling due to excessive compression at the intrados [7]. The curvature at which this maximum moment occurs, herein denoted as $\kappa_{\max}$, and its dependence on the level of external pressure is a key factor for the design of thick-walled offshore pipes [1][3].

The aforementioned works have demonstrated that initial geometric imperfections of the pipe, as well as residual stresses and material anisotropy of the steel material, induced by the line pipe manufacturing process, constitute major factors for the mechanical behavior of the steel pipe. Their magnitude depends mainly on the. In the present study, pipes manufactured by the UOE process are considered. This process consists of four sequential mechanical steps (Fig. 1): (a) crimping of the plate edges, (b) U-ing of the plate (c) O-ing of the plate and welding, and finally, (d) expansion, applying internal pressure or a mechanical expander.

The early work of Kyriakides *et al.* [8], using a simple model, has shown that the severe strain hardening, induced by cross-sectional expansion, is responsible for the degradation of ultimate pressure capacity of UOE pipes, in comparison with seamless pipes. Eight tests on 26-inch-diameter UOE pipes of 1.625 in (41.3mm) thickness and X65 steel material have been performed in support of the Oman-India pipeline [9], also reported and discussed in [3]. Two of the specimens were pressurized to collapse, and the remaining specimens were subjected to pressurized bending. Full-scale experimental testing of three UOE X65 pipes ($D/t = 45,\ 27,\ 22$) and one seamless

pipe ($D/t = 29$) accompanied by finite element simulations under external pressure and bending have been reported by Gresnigt and Van Foeken [10], [11]. The collapse pressure of the three UOE pipes was found considerably less than the one of seamless pipe [10]. On the other hand, UOE pipes had improved bending deformation capacity with respect to seamless pipes [11]. Collapse tests on 18-inch-diameter 1-inch-thick UOE pipes have been reported in [12], in an attempt to identify the effects of forming parameters on the external pressure resistance. Furthermore, a series of collapse tests and pressurized bending tests on UOE pipes have also been conducted to support the design and construction of the Mardi Gras Transportation System [13], the Blue Stream pipeline [14] and the Medgaz pipeline [15].

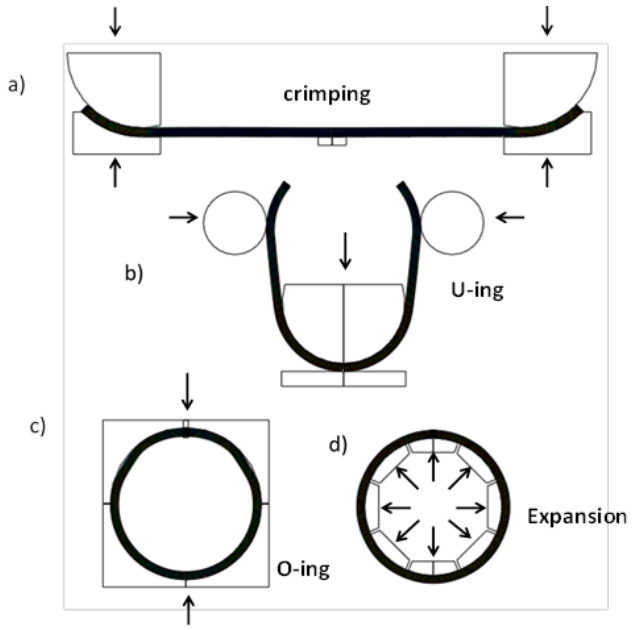

Fig. 1: Schematic representation of UOE forming steps of a steel plate: a) Crimping, b) U-press, c) O-press, d) Expansion.

In the last decade, significant effort has been devoted in modelling the UOE manufacturing process, to predict the material properties of the UOE manufactured pipe and estimate its mechanical strength under external pressure. Herynk *et al.* [16] reported a rigorous finite element simulation that follows the steps of the UOE cold bending process and the behaviour of the formed pipe subjected to external pressure, in an attempt to provide accurate predictions of the ultimate pressure capacity for a wide range of manufacturing parameters. An important modelling feature in [16] is the employment of a two-surface von Mises plasticity model, capable of modeling steel material behaviour under reverse loading conditions. Similar numerical works,

using more traditional constitutive models (isotropic or kinematic hardening) have been reported by Toscano *et al*. [17], and Varelis *et al.* [18], whereas, in a most recent publication, Tsuru and Agata [19] presented a finite element simulation of the UOE forming process using an anisotropic yield function for the steel material model.

In the present study, the cold-forming process and the mechanical behavior under combined loading conditions are simulated using a rigorous finite element model, for a UOE X70 steel pipe, candidate for deep offshore pipeline applications. The finite element model is an enhancement of the one presented in [16] to consider pressurized bending in both directions. The pipe has nominal diameter equal to 609.6 mm (24 in), and plate thickness equal to 32.33 mm (1.273 in). The material and geometric characteristics of the pipe, as well as the forming parameters are those reported in [16]. Using the present simulation, initial imperfections, residual stresses and material anisotropy of the line pipe at the end of the UOE manufacturing process are rigorously predicted, extending the findings in [16]. Following the simulation of cold-forming process, the analysis proceeds in simulating the mechanical behavior of the line pipe and determining its ultimate capacity of the pipe, subjected to (a) external pressure only, (b) external pressure in presence of axial tension, and (c) combined loading of bending and external pressure.

To model steel material behavior, a cyclic von Mises plasticity material model is developed, and implemented within the finite element model using a material-user subroutine. The model uses the nonlinear kinematic hardening rule, appropriately enhanced to account for both the yield plateau after initial yielding and the Bauschinger effect upon reverse plastic loading. A parametric analysis is also conducted with emphasis on the effects of the amount of expansion during the final stage of the UOE process, on the ultimate capacity of the pipe under combined loading conditions. Comparison between UOE and seamless pipes in terms of structural performance is also conducted. Finally, a simplified methodology is employed to estimate the capacity of the pipe, and the results are compared with those obtained from the rigorous finite element model. The numerical tools developed in the present study can be employed for optimizing the UOE manufacturing process in terms of pipe ultimate capacity under combined loading during the installation process.

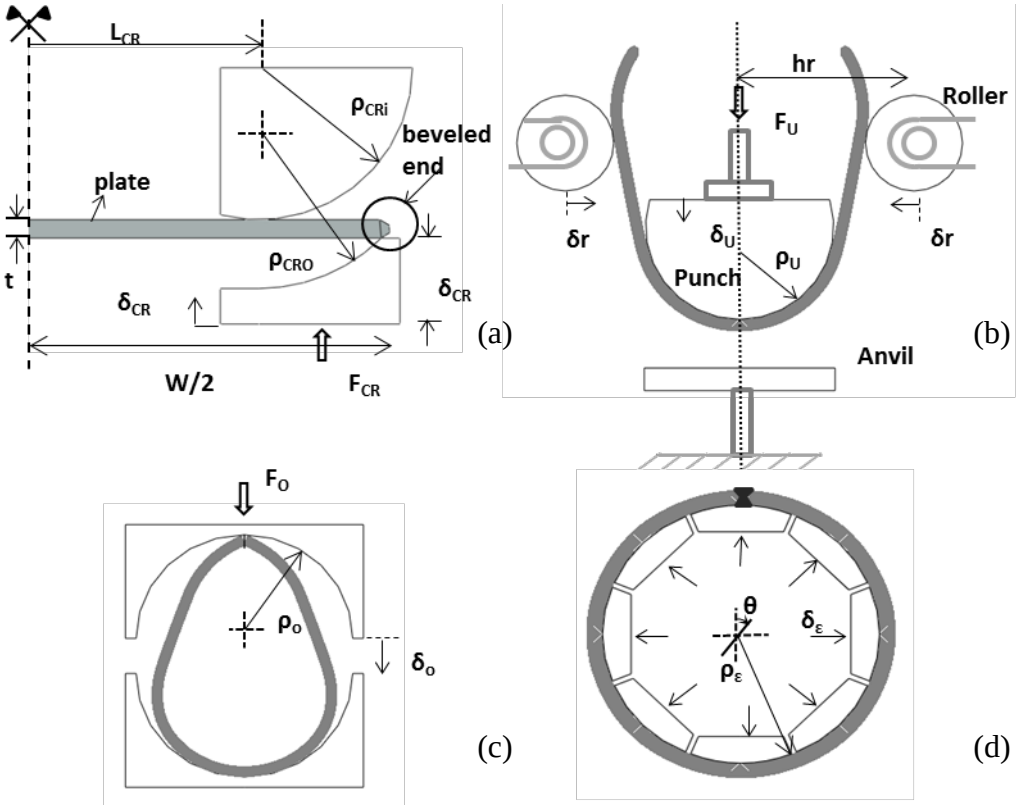

Fig. 2: Schematic representation of UOE forming phases [16]; and the corresponding parameters; (a) lower die moves upwards; (b) U-punch and side rollers displacement; (c) O-ing performed with two semi-circular dies and edge welding; (d) expansion with an eight-segment mandrel.

2 NUMERICAL MODELING

The four sequential mechanical steps (phases) of the UOE manufacturing process shown in Fig. 1 and Fig. 2 are simulated with finite elements, considering the forming parameters of Table 1. The notation of the forming parameters follows the notation in [16].

2.1 Finite element modeling description

A quasi two-dimensional model is developed in the general-purpose finite element program ABAQUS standard. The model describes the cross-sectional deformation of the pipe under generalized plane strain conditions. This allows for the simulation of both the manufacturing process from the flat configuration of the plate to the circular shape of the pipe, restraining out-of-plane displacements, as well as the subsequent application of pressure, together with tension and longitudinal bending in order to examine the structural behavior of the UOE pipe during deep-water installation. The present model considers the entire pipe cross-sections, without any symmetry, in

order to allow for the possibility of imposing bending in any direction, as explained in detail in section 4.3. A user-defined material subroutine (UMAT) is used for the description of the material behavior under severe plastic loading conditions, as presented in detail in section 2.2 and the Appendix. The pipe is discretized using four-node, reduced-integration generalized plane-strain continuum finite elements, denoted in ABAQUS as CPEG4R, whereas the forming dies for the four steps are modeled as analytical rigid surfaces. The values of the corresponding parameters of simulation are given in Table 1, and are similar to those employed by Herynk *et al*. [16]. It is important to underline that, the same finite element model is used for simulating both the manufacturing process and the subsequent application of external pressure and structural loading (tension or bending), considering an appropriate sequence of loading steps, described in the following.

The first steps of the analysis refer to the manufacturing procedure: crimping, U-ing, O-ing, welding, expansion. Each numerical step used to simulate the above manufacturing steps is followed by an unloading step to obtain the corresponding elastic rebound. For simulating the welding procedure, an additional part is assumed in the finite element model from the beginning of the analysis at both beveled ends of the plate. In order to keep the UOE process unaffected until the end of the O-ing phase, this additional part is considered elastic with a very small Young's modulus. Immediately after the O-ing phase, an additional step is performed, during which the weld material is replaced by a steel material with the appropriate Young's modulus and a yield stress 6% greater than the yield stress of the base steel material of the steel plate, corresponding to overmatched welding conditions. Moreover, special-purpose connector elements are also introduced to keep the edges of the left and the right part of the bent plate together and represent the welded pattern accurately. The connector elements are inactive until the O-ing phase is completed, and are activated immediately afterwards.

The application of external pressure and structural loading is performed in the subsequent steps of the analysis, immediately after the simulation of the manufacturing process. In the case where only external pressure is applied, the pressure load is gradually increased using Riks' continuation algorithm until the collapse pressure of the pipe is reached. In the cases where external pressure is combined with tension, tension is applied first in one step, and in the next step, keeping the tensile load constant, external pressure is increased using Riks' algorithm

until collapse. Finally, in the case of pressurized bending, external pressure is applied first in one step and, subsequently, keeping the pressure level constant, bending deformation is increased until collapse using Riks' algorithm.

Table 1: Geometric parameters of the UOE manufacturing process for the 24-inch-diameter X-70 line pipe.

	Symbol	Description	Value
Plate	t	Plate thickness (mm)	32.33
	W	Plate width (mm)	1803
	σ_y	Steel yield stress (MPa)	498
Crimping	ρ_{CRi}	Internal crimping radius (mm)	265.4
	ρ_{CRo}	External crimping radius (mm)	298.5
	δ_{CR}	Final distance of the 2 dies (mm)	0.5
	L_{CR}	Horizontal distance of the dies (mm)	676.7
	h_{CR}	Height of the external crimping die (mm)	150
U-ing	ρ_U	U-Punch radius (mm)	246.4
	δ_U	Distance covered by the U-Punch (mm)	724
	δ_r	Distance covered by the Roller (mm)	102
	h_r	Horizontal Roller position (mm)	457
	υ_r	Vertical position of the Anvil (mm)	724
O-ing	ρ_O	Radius of the semi-circular dies (mm)	303.8
	δ_O	Overlap of the O-dies centers (mm)	0
Expansion	ρ_E	Mandrel radius (mm)	260
	δ_E	Expansion value (mm)	7.75
	N_E	Number of mandrel segments	8

2.2 Constitutive modeling

The accurate simulation of material behavior under reverse loading conditions is of major importance for modeling the UOE process and for the reliable prediction of line pipe structural capacity. In the course of UOE manufacturing process, the pipe material is deformed well into the plastic range, so that reverse loading is characterized by the appearance of the Bauschinger effect. In the present study, the elastic-plastic behavior of the steel pipe material is described through a von Mises plasticity model with nonlinear kinematic hardening, properly enhanced to describe both the yield plateau of the steel stress-strain curve upon initial yielding and the Bauschinger effect under reverse plastic loading.

The constitutive model considers a nonlinear kinematic hardening rule, initially proposed in [20], enhanced for the purposes of the present work, whereas the size of the yield surface is a function of the equivalent plastic strain. Furthermore, an enhancement of the model, proposed elsewhere [21], is introduced to account for the abrupt change of shape in the stress-strain curve after initial yielding (plastic plateau). The material model has been implemented in a user-subroutine (UMAT) for ABAQUS/Standard, using an "elastic predictor – plastic corrector" (Euler- backward) numerical integration scheme. More details on the constitutive model and its numerical implementation are offered in the Appendix, as well as in [22].

The model is calibrated with a stress-strain curve from uniaxial testing of a steel coupon as shown in Fig. 3 extracted from the steel plate before the UOE manufacturing takes place [16]. The yield stress of steel material σ_y is equal to 498 MPa (72 ksi), corresponding to X-70 steel grade. The capability of the present material model to reproduce the experimental uniaxial stress-strain curve of the X-70 steel is shown in Fig. 3; both the plateau region after initial yielding and the Bauschinger effect are described satisfactorily. It is worth noticing that this test in [16] has indicated a reduced value of Young's modulus E during unloading. The influence of this reduced value of E on pressure capacity can be taken into account through an appropriate enhancement of the constitutive model, and this influence will be examined in a later section of the present paper.

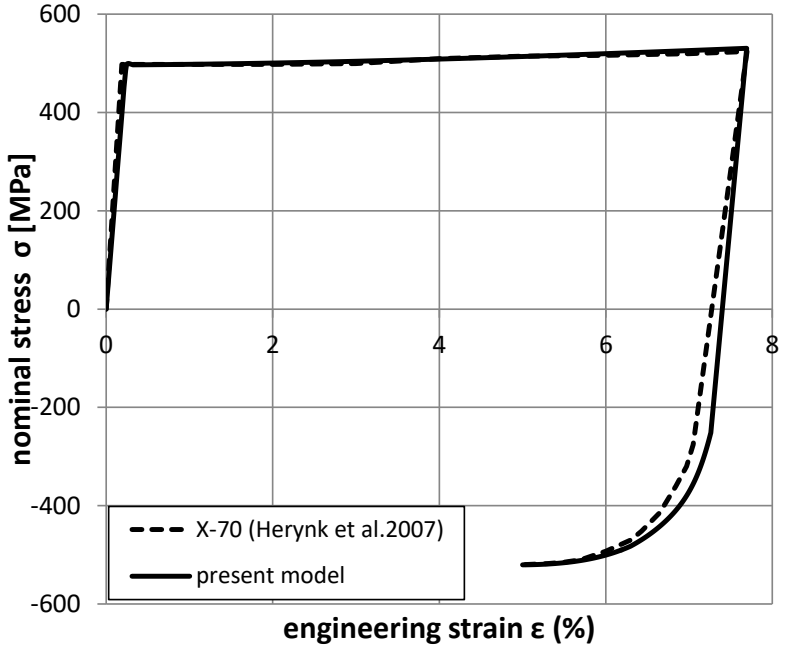

Fig. 3: Test and material modeling for uniaxial X-70 stress – strain curve [16].

3 NUMERICAL RESULTS FOR UOE MANUFACTURING PROCESS

Results are reported for a pipe with external nominal diameter equal to 24 inches (609.6 mm). The plate width and thickness are 1803 mm (70.98 in) and 32.33 mm (1.273 in) respectively, as shown in Table 1. The parameters of the UOE cold forming process simulation are also presented in Table 1 and are similar to those considered in Herynk *et al.* [16]. In Fig. 4 to Fig. 7, pipe configurations at different stages of the UOE process are shown and the color contours represent the distribution of von Mises stress. Special emphasis of the numerical simulation is given on the variation of out-of-roundness and thickness reduction around the pipe cross-section.

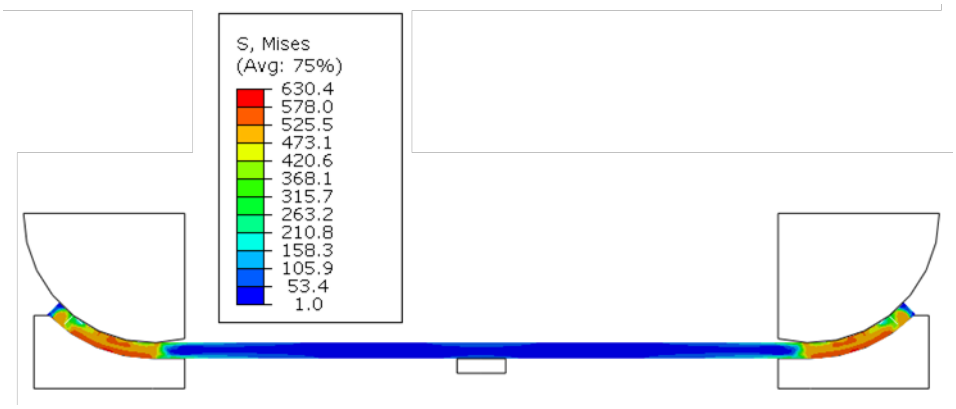

Fig. 4: Plate configuration at the end of the crimping process.

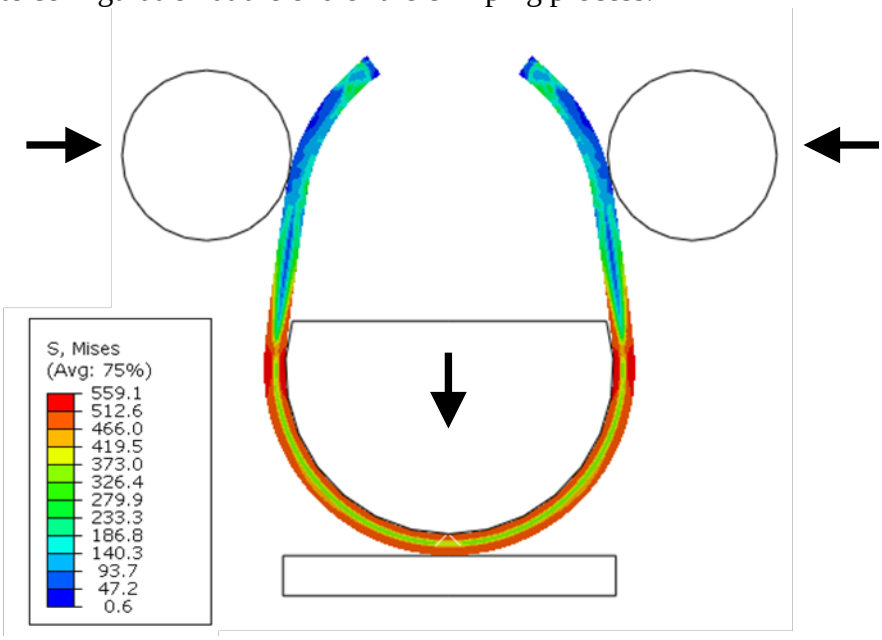

Fig. 5: Numerical simulation of plate deformation during the U-ing process.

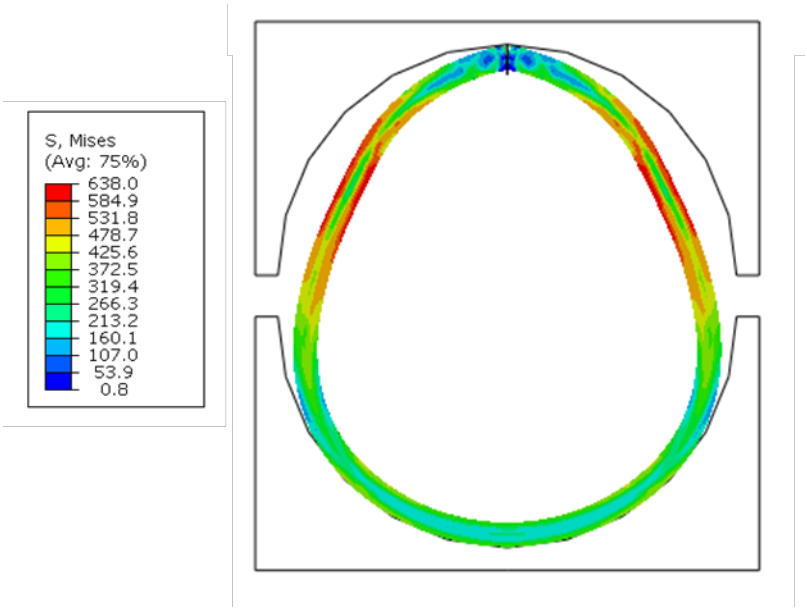

Fig. 6: Plate configuration during the O-ing process at the stage where the two beveled ends come together.

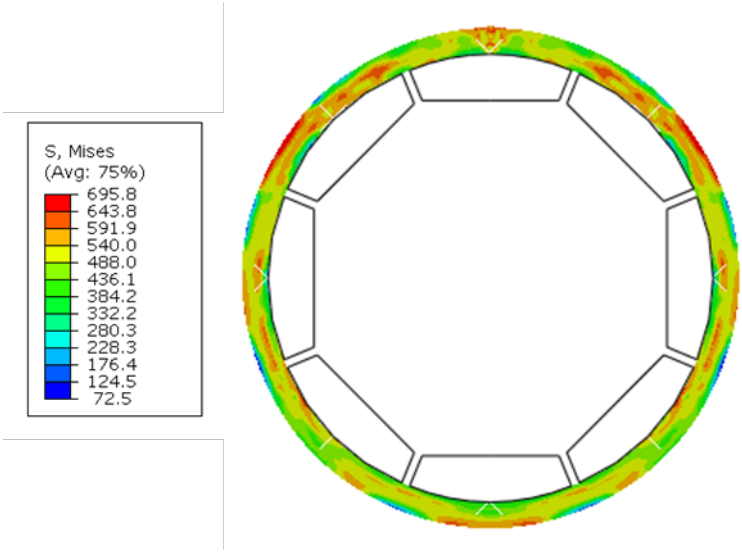

Fig. 7: Pipe configuration during the expansion process; all mandrels are displaced simultaneously by the same amount in the radial direction.

During the numerical simulation of the manufacturing process, the value of the expansion displacement constitutes a key parameter. In the present work, the expansion value is considered equal to zero at the point where the first mandrel reaches contact with the inner surface of the pipe. This is referred to as “UO” case. After the stage of first contact, the mandrels accommodate themselves within the pipe interior causing expansion and bending deformation on the pipe wall. At the stage where all mandrel segments are in contact with the pipe walls, the pipe has reached a

quasi-rounded shape. Upon increased outward displacement of the mandrels, the circularity of the pipe is further improved. This outward movement of the mandrels induces net hoop strain represented by the "expansion hoop strain" parameter, denoted as ε_{E} and defined by the following equation:

$$\varepsilon_{\mathrm{E}} = \frac{C_E - C_O}{C_O} \tag{1}$$

where C_E and C_O are the mid-surface lengths of the pipe circumference after the expansion phase and after the O-ing phase (UO case) respectively, also adopted in [16] and [18]. Note that the value of C_E is measured after the mandrels are removed, therefore it may be considered as a "permanent" expansion hoop strain, which accounts for the small "elastic rebound". It should also be noted that this "expansion hoop strain: is quite different than the local hoop strain of the pipe material after the UOE process; the value of ε_{E} should be considered as a "macroscopic" parameter to quantify the size of expansion. Fig. 8 depicts the relation between the value of expansion displacement u_{E} and the corresponding permanent expansion hoop strain ε_{E}. In the present analysis, the value of u_{E} ranges from u_{E}=0 mm (UO case) to u_{E} =8.35 mm, (ε_{E} equal to 1.17%). Fig. 8 shows that the permanent expansion hoop strain ε_{E} is a non-linear function of the expansion displacement u_{E}.

3.1 Line pipe ovalization and out-of-roundness

An important parameter for assessing the mechanical behavior of offshore pipes subjected to external pressure is the ovalization of pipe cross–section after the manufacturing process, also referred to as "cross-sectional ovality". Ovalization is a geometric imperfection of the pipe and may have a significant effect on the ultimate capacity under high external pressure, causing premature collapse.

To quantify pipe cross-section ovality, the ovality parameter Δ_0 is defined as follows:

$$\Delta_0 = \frac{|D_1 - D_2|}{D_1 + D_2} \tag{2}$$

where D_1 and D_2 are the horizontal and vertical outer diameters of the pipe cross-section respectively, measured at the end of the UOE process.

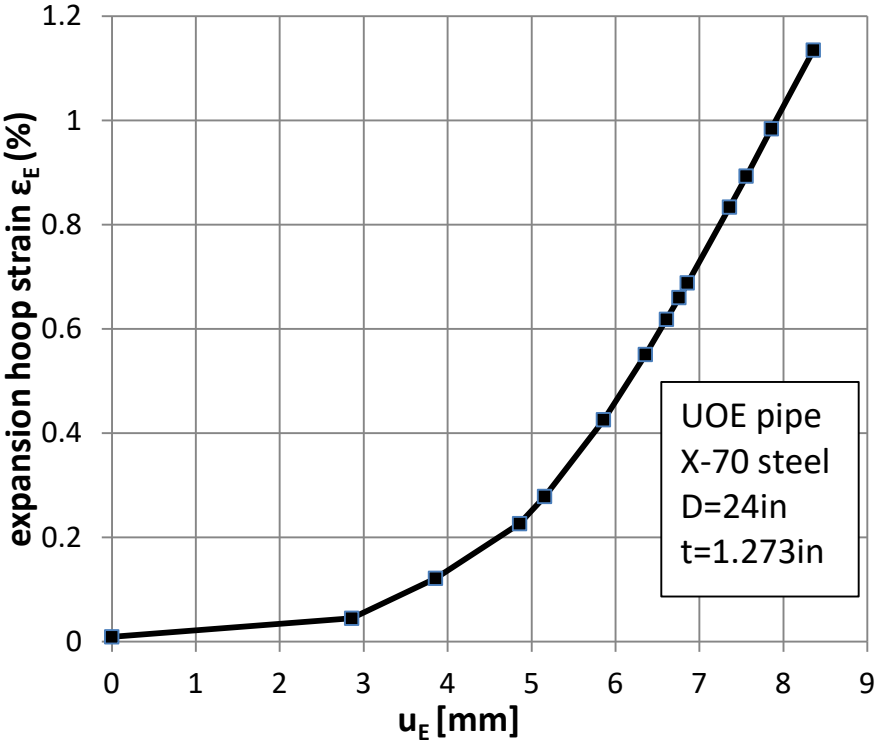

Fig. 8: Variation of the induced (permanent) hoop expansion strain ε_E in terms of the expansion displacement value u_E of the formed UOE pipe.

The effect of expansion hoop strain ε_E of the UOE pipe under consideration on the ovalization parameter Δ_0, defined by Eq. (2), is illustrated in Fig. 9. As the expansion increases, the value of the ovality parameter drops rapidly and obtains quite small values (less than 0.2%) for expansion strains equal to about 0.3%. Further increase of the applied expansion hoop strain ε_E causes additional decrease of ovalization. In addition, the expansion improves pipe roundness alleviating the "shoulders", which appear after the O-phase and are primarily responsible for the non-circularity of the UO pipe, as shown in Fig. 10. The two shoulders are formed during the O-phase under the upper semi-circular die. Fig. 10a depicts the shape of a pipe (UO case), where the two shoulders occur at angle θ equal to about $\pm$ 45°, while the location of the weld corresponds to θ equal to 0°. On the other hand, Fig. 10b refers to the UOE case with the highest expansion hoop strain considered (ε_E = 1.17%). In latter case, due to significant expansion, the two "shoulders" have disappeared. The results are illustrated graphically in Fig. 11 in terms of the difference between the value of the radius r at a specific location θ around the cross

section circumference and the average radius r_{ave} ($\Delta r = r - r_{ave}$). The plots indicate that, for small expansion values, a significant deviation from circularity occurs. However, as expansion increases, pipe circularity improves and, consequently, the value of Δr decreases.

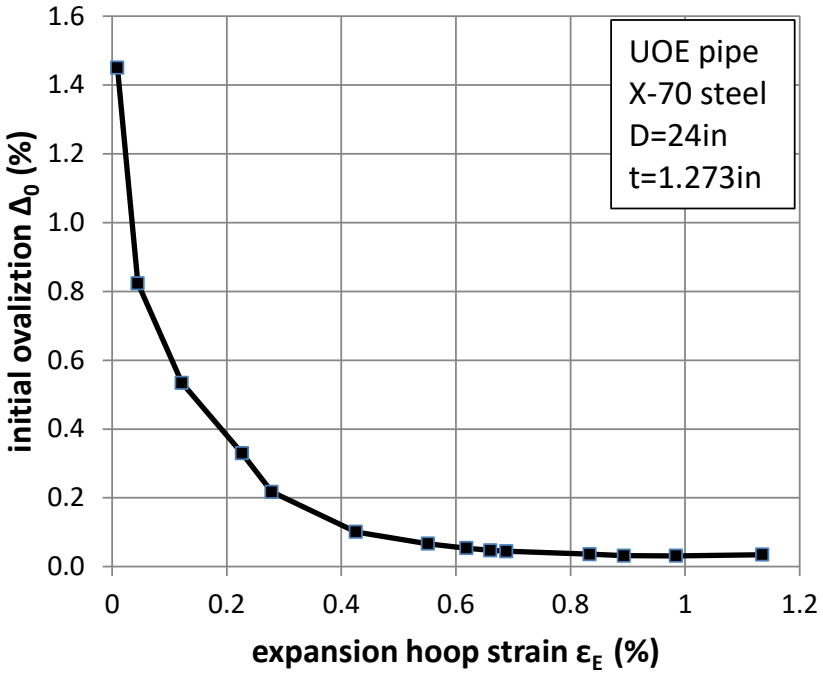

Fig. 9: Ovality parameter in terms of permanent expansion hoop strain.

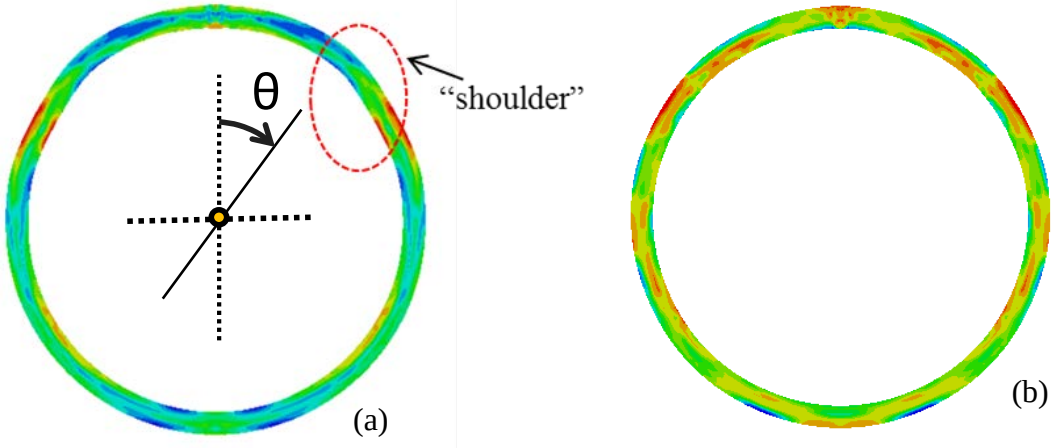

Fig. 10: Pipe cross-sectional shapes obtained from finite element analysis:(a) UO case ($\varepsilon_E = 0\%$), (b) UOE case with $\varepsilon_E = 1.17\%$.

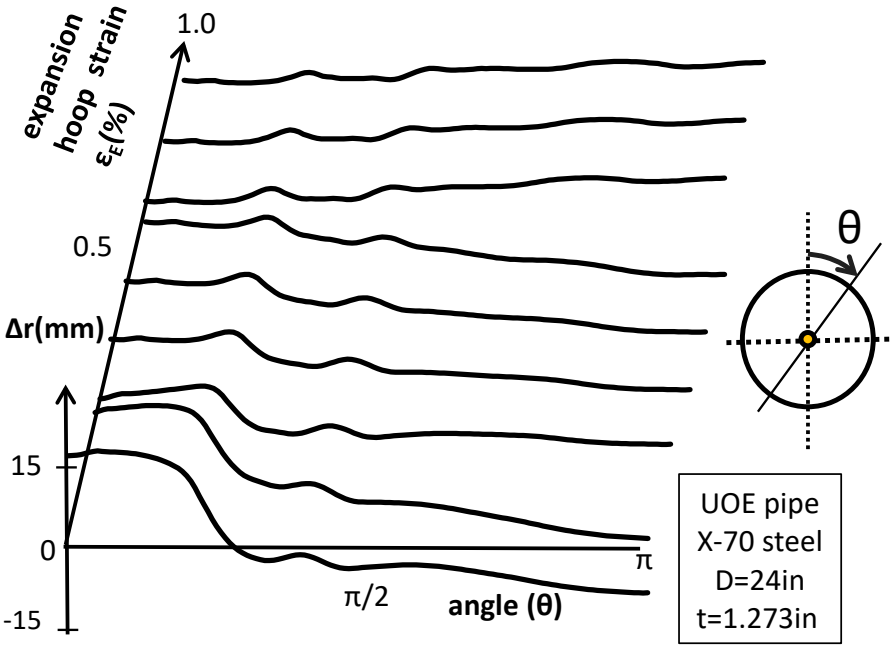

Fig. 11: Effect of expansion hoop strain on the roundness of the pipe expressed in terms of local radius variation $\Delta r = r - r_{ave}$.

3.2 Line Pipe Thickness

Due to the manufacturing process, the thickness of a UOE pipe after forming is different than the original thickness of the initial steel plate. The numerical results have shown that the mean (average) thickness of the pipe t_{ave} around the cross-section, computed at the end of the UOE process (including unloading), decreases with increasing values of hoop expansion ε_{E} in a quasi-linear manner. More specifically, the average thickness for a pipe with zero expansion $\varepsilon_{\mathrm{E}} = 0\%$, corresponding to the UO case, is equal to 32.29 mm, very close to the original plate thickness, whereas for $\varepsilon_{\mathrm{E}} = 1\%$ the average thickness reduces to 31.96 mm, corresponding to a 1.15% reduction with respect to the initial plate thickness. To quantify variations of thickness around the pipe cross-section, a non-dimensional thickness imperfection parameter is introduced, denoted as $\Delta\mathrm{T}$, which expresses the variation of the circumferential pipe wall thickness as follows:

$$\Delta T = \frac{t_{\max} - t_{\min}}{t_{ave}} \tag{3}$$

In the above equation, $t_{\max}$ is the maximum value of thickness measured around the circumference at the specific cross section and $t_{\min}$ is the corresponding minimum

value, both measured considering the entire circumference of the cross-section, except for the weld location. Fig. 12 shows the thickness variation parameter ΔT for various values of ε_{E}. The increase of the ΔT value is due to the reduction of thickness at higher levels of expansion and mainly in the area of the "shoulder".

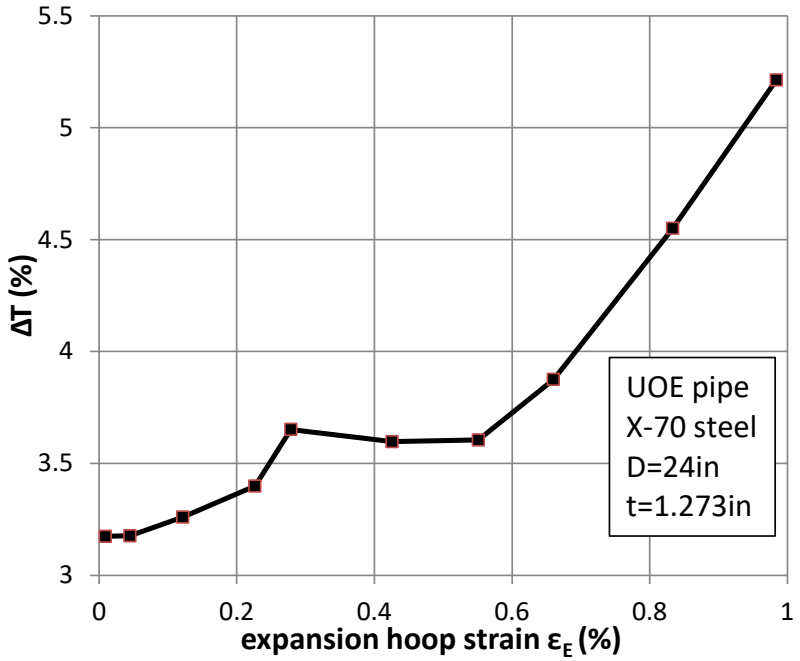

Fig. 12: Effect of expansion hoop strain on thickness imperfection parameter of the formed UOE pipe.

3.3 Manufacturing-induced anisotropy of the steel material

The UOE forming process introduces significant stresses and deformations, the material enters the strain hardening region and, consequently, its initial stress–strain response is modified and anisotropy is introduced. In practice, the anisotropy at the end of the UOE forming process is evaluated by extracting two strip specimens from the longitudinal and hoop direction of the pipe, and subjecting them to uniaxial tension and compression respectively, so that the corresponding stress-strain curves in each direction are obtained [3].

A numerical simulation of this experimental procedure is attempted in the present study. More specifically, two locations located at angles of 90º and 180º from the weld region are considered and at each location two integration points are selected, one at the external surface of the pipe and the other at the internal surface. Throughout the forming process all material state parameters (stresses, strains) are recorded at those integration points. Subsequently, a "unit cube" finite element model is

considered and the material parameters from each integration point are introduced as initial state variables of this unit cube model and a first analysis step with zero external loading is performed, simulating the extraction of the strip specimen from the pipe. At this first step, the residual stresses are reduced to zero but the plastic deformations due to the forming process are maintained. In addition, a second step is performed where the "cube" is loaded under uniaxial compression in the hoop direction of the pipe or under uniaxial tension in the direction parallel to the pipe axis. The average response of the integration points in each direction represents the mechanical behavior of the pipe material at this specific direction. Representative results of this analysis are shown in Fig. 13 in terms of the stress-strain response of an expansion hoop strain ε_{E} value equal to 1%. Considering that the axial tensile curve represents the fundamental response of the material, the different behavior in the hoop direction is quantified in terms of the following anisotropy parameter:

$$S = \frac{\sigma_{Y\theta}}{\sigma_{Yx}} \tag{4}$$

where σ_{Yx} is the yield stress in the pipe axial direction and $\sigma_{Y\theta}$ is the circumferential yield stress of the pipe. Fig. 14 depicts the anisotropy parameter for various values of the expansion hoop strains and indicates that increasing expansion hoop strain, the induced material anisotropy increases. The values of the anisotropy parameter ranges from 0.98 for zero expansion to 0.90 for significant expansion hoop strain values $(\varepsilon_{\mathrm{E}} = 1\%)$. In all cases, the compressive yield stress in the hoop direction is lower than the corresponding tensile yield stress in the longitudinal direction of the pipe.

4 NUMERICAL SIMULATION OF THE STRUCTURAL BEHAVIOR OF UOE PIPES

Following the simulation of the forming process, the UOE pipe under consideration is subjected to loading conditions which stem from their installation procedure in deep water. In paragraph 4.1, the response and the ultimate capacity under external pressure is examined, whereas paragraph 4.2 focuses on the effect of tension on the pressure capacity. Finally, in paragraph 4.3 the bending response of UOE pipes in the presence of external pressure is investigated. The values of pressure P, moment M, tension T and curvature κ, used in the following sections, are normalized by the yield pressure $P_y = 2\sigma_Y t/D_m$, the fully plastic moment $M_P = \sigma_Y D_m^2 t$,

the yield tension $T_y = \pi\sigma_Y D_m$ and the curvature parameter $\kappa_1 = t/D_m^2$ respectively, where D_m is the mean pipe nominal diameter ($D_m = D - t$) and t is the nominal thickness.

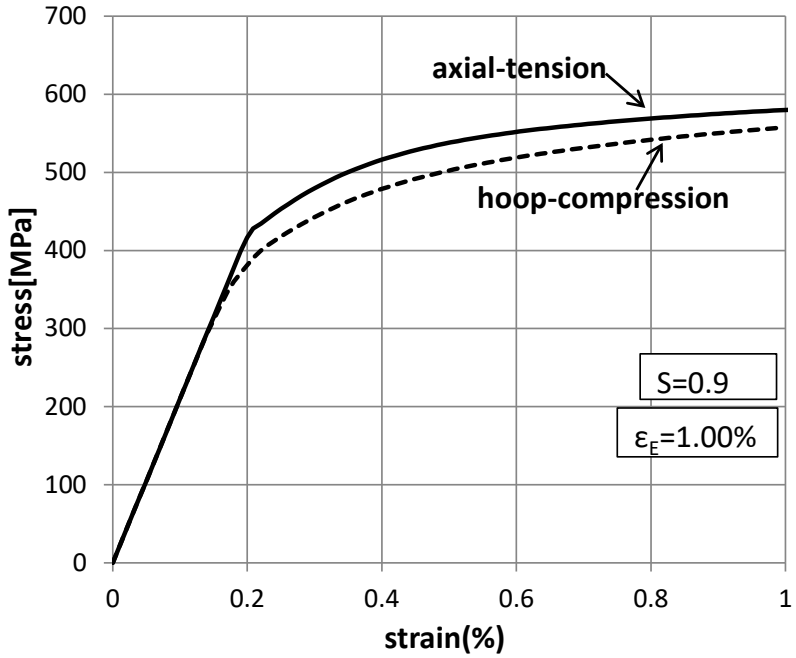

Fig. 13: Comparison of the average axial tensile and circumferential compressive responses for values of hoop expansion strain ε_E equal to 1.0%.

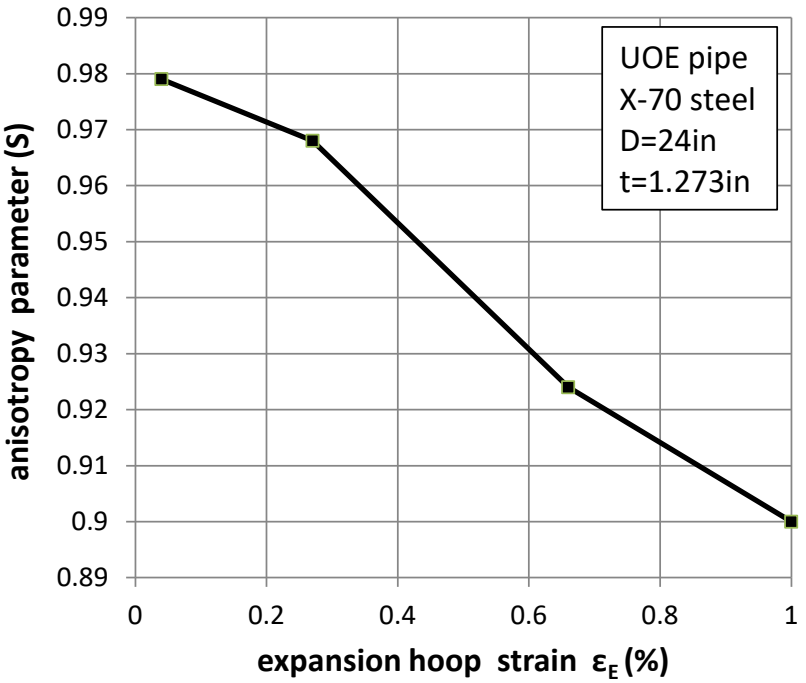

Fig. 14: Variation of anisotropy in terms of the expansion hoop strain ε_E.

4.1 Behavior under external pressure

Each of the forming parameters of the UOE manufacturing process has an important effect on the response of UOE pipes under external pressure. An extensive investigation of the influence of each parameter on the ultimate pressure capacity is offered in [16]. In the present section, the effect of expansion phase on the ultimate pressure is examined through a short parametric analysis. This constitutes a first step towards evaluating the results presented in subsequent sections 4.2, 4.3 on the capacity under combined loading conditions. In Fig. 15, the predicted collapse pressure of the pipe under consideration, denoted as P_{CO}, is presented with respect to the applied expansion hoop strain ε_{E} with the solid curve. Starting from the UO case ($\varepsilon_{\mathrm{E}} = 0\%$), the initial ovality drops sharply with increasing value of ε_{E}, as shown in Fig. 9, resulting to an increase of P_{CO}, shown in Fig. 15. One should note that at relatively small values of ovalization corresponding to expansion hoop strains greater than 0.61%, significant residual stresses are induced by the cold-forming process, resulting to a decrease of the maximum collapse pressure, attributed to the reduction of the corresponding compressive strength of the material due to the Bauschinger effect. The failure mode obtained for ε_{E} values up to 0.68% is cross-sectional ovalization with flattening in the direction of the vertical plane (θ=0°) denoted as and shown in Fig. 16. For larger values of expansion the failure mode is also cross-sectional ovalization and can be either flattening in vertical plane or flattening of the horizontal plane , shown in Fig. 17 depending on the initial imperfections. Note that the post-buckling configuration of both flattening modes is non-symmetric with respect to θ=90° plane due to the presence of the weld. Fig. 18 shows the response of pressurized pipes in terms of a pressure-ovalization diagram and the dependence of maximum pressure on the amplitude of initial ovalization. Until the pipe reaches its maximum pressure, the ovalization is small, as shown in stage (a) of Fig. 16. When the pipe buckles, the cross-sectional shape corresponds to state (b) in Fig. 16 with higher ovalization. After that stage the ovalization continues to increase and the corresponding pressure decreases further.

The numerical results show that for the case under consideration, a maximum value of P_{CO} is reached at a value of ε_{E} equal to about 0.66% (Fig. 15), after which further increase of ε_{E} progressively reduces P_{CO}. Therefore, there exist an optimum

expansion at which the highest resistance against external pressure instability (buckling) is achieved, an observation consistent with the one reported in [16]. The corresponding value of optimum expansion reported in [16] is significantly lower (0.30%), and this difference is due to the lower value of Young's modulus during unloading observed in the experiment of Fig. 3, which has been taken into consideration in the analysis of Herynk *et al.* [16]. In the present work, to account for this reduction, the constitutive model is enhanced, assuming that the value of E is a function of the equivalent plastic strain ε_q as follows:

$$E = E_0 - \Delta E\left(1 - e^{-\xi\varepsilon_q}\right) \tag{5}$$

In equation (5), E_0 is the initial Young's modulus, and parameters ΔE, ξ are chosen equal to 49 GPa and 30 respectively, so that the experimental curve of Fig. 3 is exactly reproduced. Using the above modification, the dotted line of Fig. 15 is obtained, showing maximum pressure capacity at about 0.32%, which is a result very close to the one reported in [16].

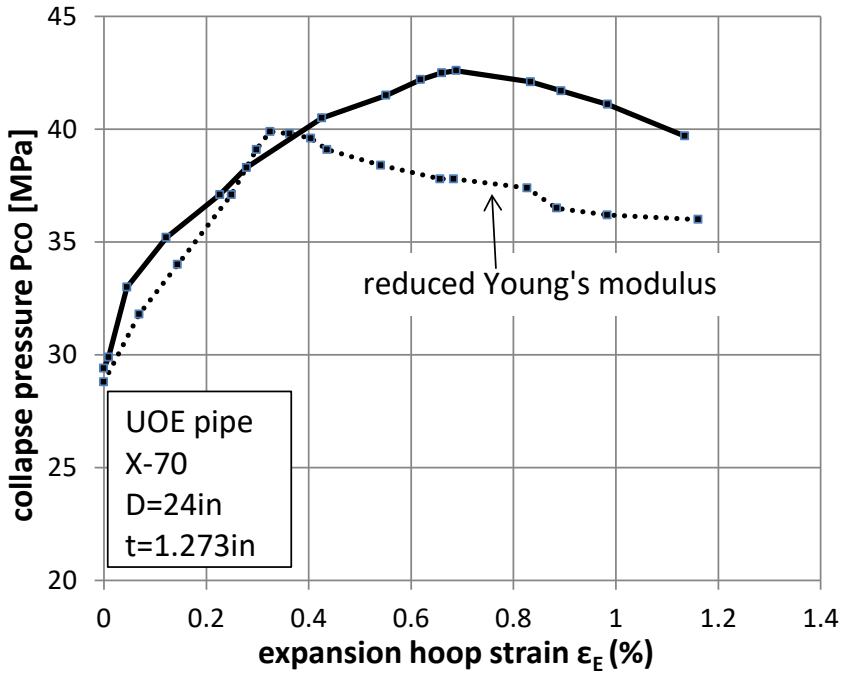

Fig. 15: Variation of collapse pressure with respect to the expansion hoop strain ε_{E}.

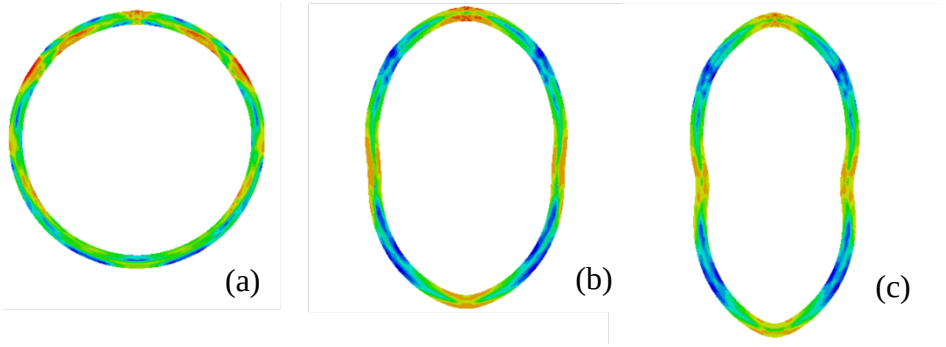

Fig. 16: Deformed shape of the UOE pipe under external pressure for expansion hoop strain ε_E equal to 0.27%; cross-sectional flattening in the vertical direction ⬯.

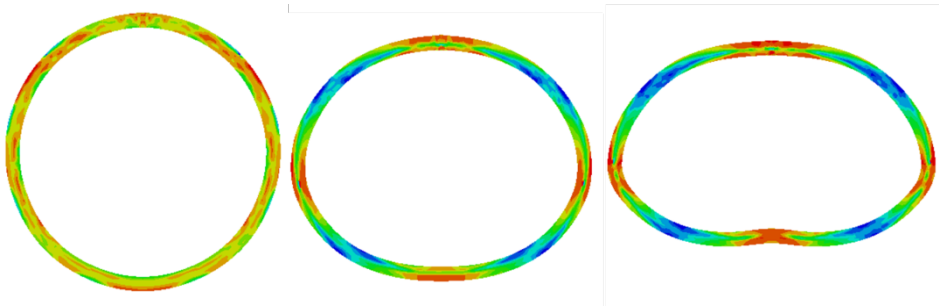

Fig. 17: Deformed shape of UOE pipe under external pressure for expansion hoop strain ε_E equal to 1.00%; cross-sectional flattening in the horizontal direction ⬭.

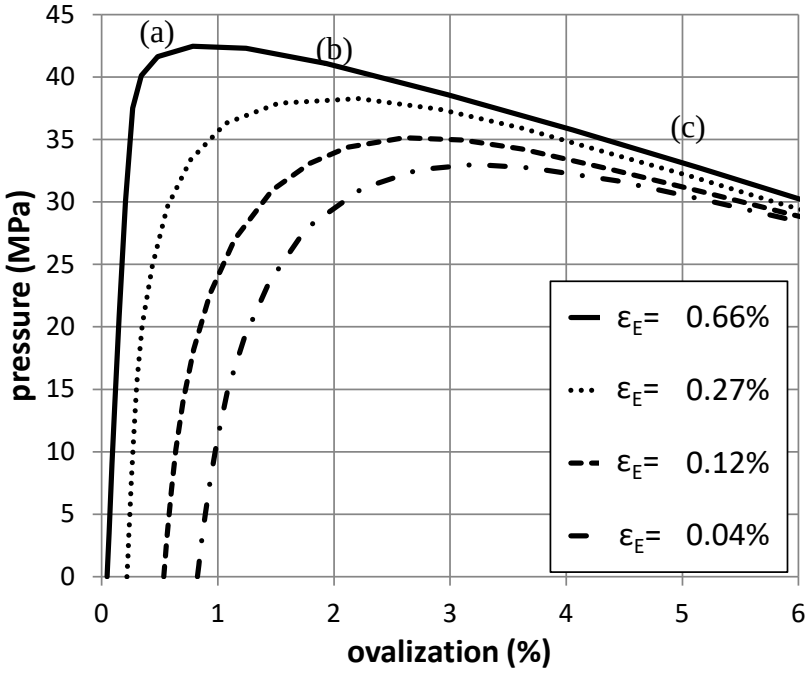

Fig. 18: Response of UOE pipes under external pressure for different values of expansion strain corresponding to different values of initial ovalization.

The behavior of a seamless pipe with the same geometric and material characteristics is also considered for comparison purposes. The seamless pipe has the

same nominal diameter and thickness (24 in and 1.273 in) and the material properties of the steel plate (virgin material). Initial ovalization is introduced as an initial geometric oval shape of the cross-section, and the pipe is free of any residual stresses or strains. This stems from the fact that seamless pipes have negligible residual stresses and strains at the end of their manufacturing process. In Fig. 19 the behavior of the seamless pipe under external pressure is compared with the corresponding behavior of the UOE pipe. The seamless pipe can sustain higher pressure than the corresponding UOE pipe with the same ovalization. This difference ranges from about 30% for small initial ovality values (large expansion) to about 18% for higher ovality (small expansion).

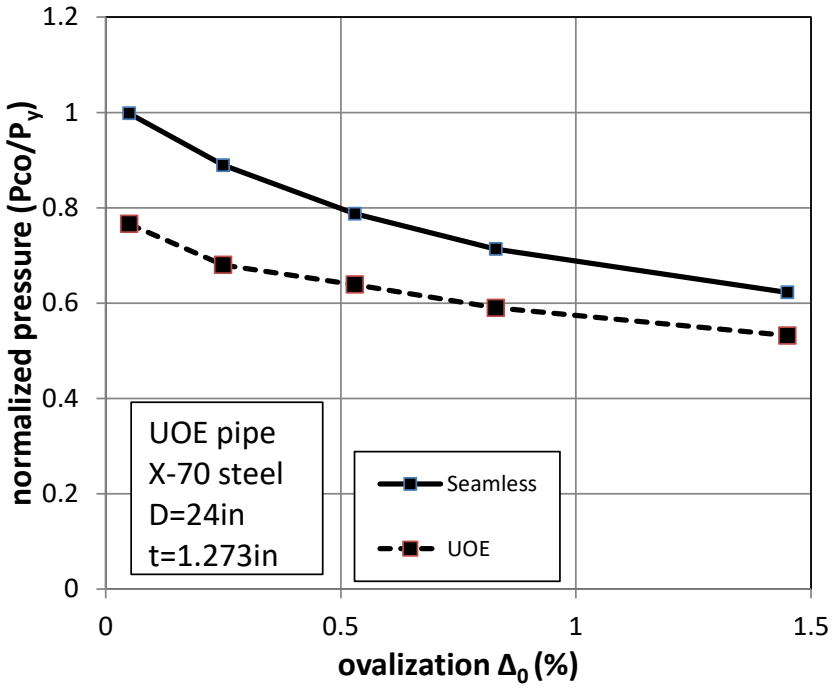

Fig. 19: The effect of initial ovalization on the collapse pressure of UOE and seamless pipes.

4.2 The effect of tension on external pressure capacity of UOE pipes.

During deep-water the installation, at about mid-depth, the pipeline undergoes a loading pattern which consists of the combined action of external pressure and axial tension. It is expected that as tension increases, the collapse (ultimate) pressure decreases due to the earlier yielding in the hoop direction, as calculated from the von Mises yield criterion [3] [4]. In the present paragraph, the influence of tensile force on pressure capacity of UOE pipes is examined. Following the finite element simulation of the UOE process, the pipes are subjected to combined tension and pressure,

according to the loading sequence described in section 3: a prescribed level of tension force is applied first and subsequently, keeping the tension force constant, external pressure is applied until collapse of the pipe occurs. Fig. 20 illustrates the behavior of three UOE pipes with different expansions ($\varepsilon_E = 0.04\%$, $\varepsilon_E = 0.27\%$ and $\varepsilon_E = 0.66\%$) under combined tension and external pressure loading. The results indicate that the resistance against external pressure decreases as the applied tension increases. Furthermore a comparison between seamless and UOE pipes is conducted and the corresponding interaction diagrams in Fig. 21 show that for low levels of tensile force, seamless pipes have higher resistance against external pressure. This is also shown in Fig. 22 for the response of a UOE pipe and the corresponding seamless pipe under external pressure for tensile force equal to 20% of yield tension. On the contrary, for higher levels of tensile force, exceeding 50% of the yield tension, UOE pipes exhibit better behavior under external pressure than the corresponding seamless pipes. This is attributed to the strain hardening of the material induced by the UOE manufacturing process, resulting in an increased yield strength with respect to the yield stress of the seamless pipe.

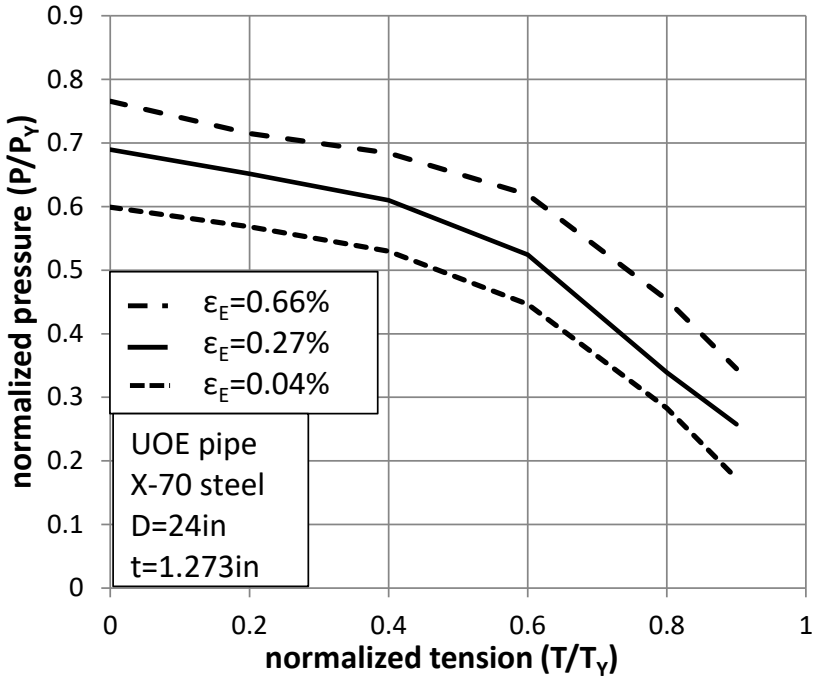

Fig. 20: Tension-pressure interaction diagram ($T \rightarrow P$) for three UOE pipes with expansion hoop strains ε_E equal to 0.04%, 0.27% and 0.66%.

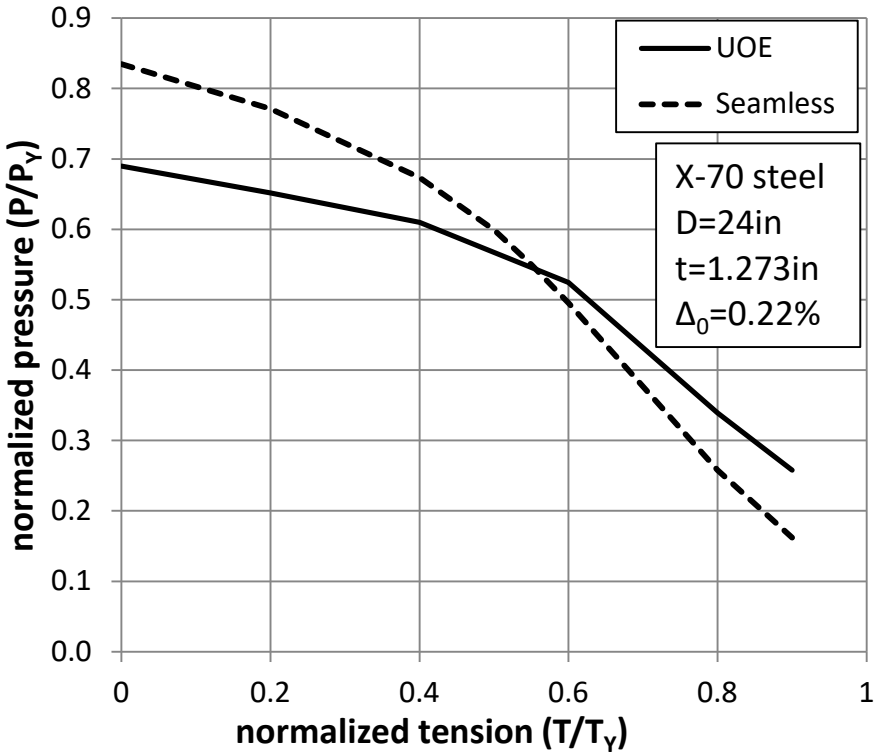

Fig. 21 Tension-pressure interaction diagram ($T \rightarrow P$); comparison between seamless and UOE pipe with initial ovality Δ_0 equal to 0.22%.

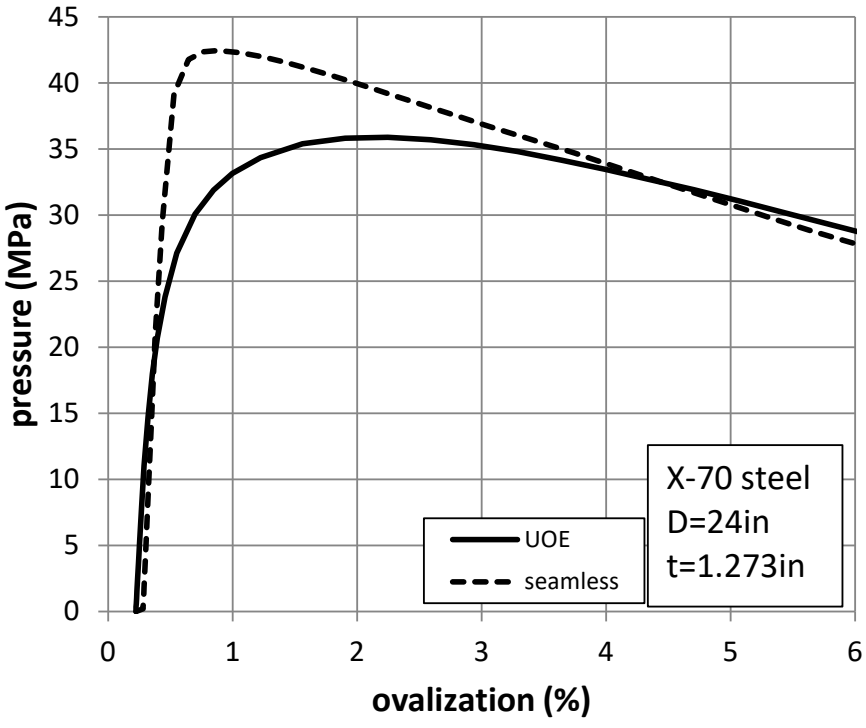

Fig. 22: Response of a UOE pipe and the corresponding seamless pipe under external pressure, for tensile force equal to 20% of the yield axial force ($T/T_Y = 0.20$).

4.3 The effect of forming process on the pressurized bending capacity of UOE pipes

During the installation process, the external pressure applied on the pipe causes buckling in the form of cross-sectional ovalization. As the pipe approaches the sea bed (sagbend region), it is also subjected to bending also associated with the development of cross-sectional ovalization which interacts with the ovalization due to pressure and may result in premature collapse. The interaction of bending with external pressure is a key design issue for an offshore pipeline. To analyze this interaction a pressure-curvature loading sequence is considered using the developed model as follows: pressure is applied first and subsequently, keeping the pressure constant, the pipe is subjected to bending. This loading sequence has been also described in section 3 and it is referred to as $P \rightarrow \kappa$ loading path. An important observation refers to the direction at which bending is applied. In practice, bending can be applied at any direction with respect to the weld location. Therefore, to consider the worst-case scenario, bending should be applied at the plane where bending ovalization is added to the ovalization due to pressure. Thus, it is necessary to identify for the specific value of ε_E the corresponding buckling mode due to external pressure ( or ) and apply bending at the direction that represents the worst-case scenario. Following this argument, in cases where external pressure buckling occurs in mode  , bending should be applied in the θ=90º plane, therefore a model which is symmetric with respect to θ=0º plane cannot be adopted. This is the main reason for considering the full model, without any symmetry conditions as described in section 3. If bending is applied in any other direction, the bending capacity of the pipe under pressurized conditions would be significantly higher due to the fact that pressure ovalization would counteract bending ovalization.

Due to the deformation-controlled conditions in the course of the installation procedure, the "critical curvature" of the bent pipe, denoted as κ_{max}, is a parameter of paramount importance. There exist several definitions of this "critical curvature". In the case of thick-walled pipes, used in deep-water applications, bending response is characterized by limit moment instability due to ovalization. Therefore, the curvature at which the maximum moment M_{max} occurs as a result of ovalization instability can be considered as the "critical curvature" κ_{max} for the UOE pipes under consideration. In the present analysis, after the simulation of the forming process, an additional step

is performed so that the UOE pipes are subjected to a prescribed level of uniform external pressure and, in the final step, keeping the pressure constant, curvature-controlled bending is applied until the pipe reaches its maximum moment resistance. The corresponding curvature is the "critical curvature" of interest. For each case examined, corresponding to different expansion values, bending is applied in the appropriate direction depending on the failure mode of the pipe under external pressure as noted above. Fig. 23 depicts the effect of expansion strain ε_E on the bending deformation capacity of UOE pipes in the presence of low and moderate pressure level ($P/P_y = 0.09$ and 0.36). The results show that for the case of low pressure level, the critical curvature κ_{max} remains nearly unaffected with respect to the ε_E value. On the other hand, for moderate level of pressure, the value of κ_{max} increases with increasing values of the expansion hoop strain ε_E.

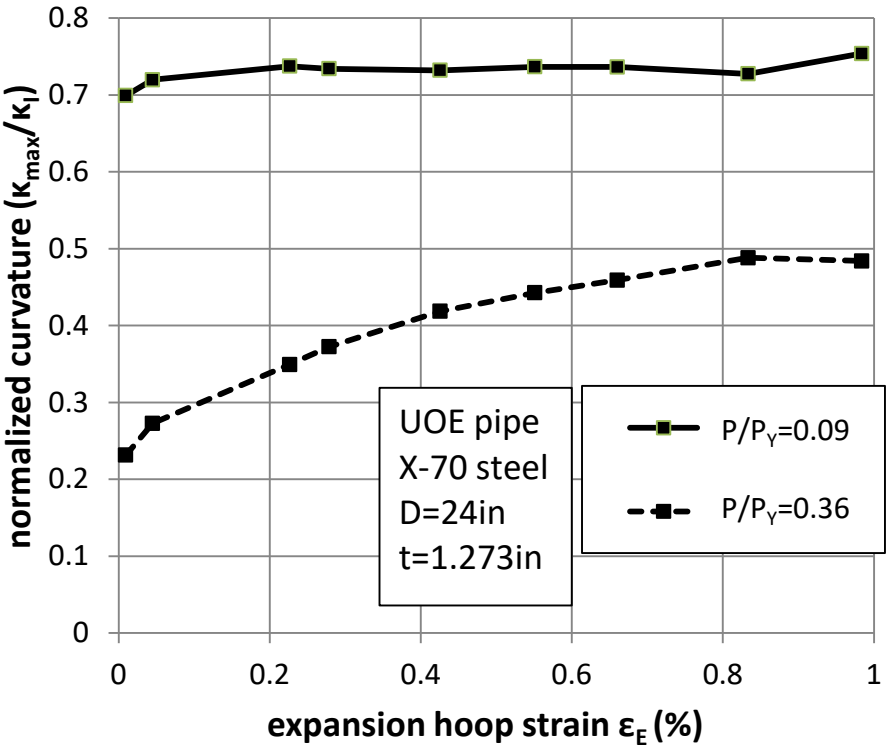

Fig. 23: Variation of critical curvature κ_{max} with respect to expansion hoop strain ε_E, for two levels of external pressure (9% and 36% of the yield pressure).

During the UOE cold bending, the pipe material is strained well into the plastic range and this is associated with significant strain hardening. The numerical results show that this is beneficial for the bending capacity of UOE pipes under zero

pressure. Gresnigt and Van Foeken [11] reported the same conclusions based on the results of their experimental investigation. On the other hand, the presence of external pressure causes significant compressive stresses in the pipe. In this case, the influence of the Baushinger effect becomes important resulting in a reduction of pipe bending capacity. The effect of the UOE manufacturing process on the pressure-curvature interaction curve for pipes with three different expansions is depicted in Fig. 24 and Fig. 25. For relatively high levels of external pressure, there is a quasi-linear reduction of bending deformation also observed in the pressurized bending tests reported in [9]. In each case, the behavior is compared with the behavior of a seamless pipe which has the same geometrical and material characteristics with the UOE pipe.

Comparison of the numerical results shows that UOE pipes have a significantly different behavior compared to seamless pipes. More specifically, for small values of external pressure, the UOE pipe is capable of reaching higher curvature than the seamless pipe. On the contrary, at higher pressure levels, seamless pipe bending response is associated with larger values of maximum curvature $\kappa_{\max}$. This is attributed to the fact that the UOE manufactured pipe has a significantly reduced pressure capacity compared with a similar seamless pipe, also noted in [10]. Seamless pipes are associated with negligible residual stresses, and therefore they exhibit lower initial yield strength, but are free of the Bauschinger effect. On the other hand there is a beneficial effect of the UOE process on the bending capacity of the pipe, also noted in [11].

Fig. 26 to Fig. 29 depict the moment-curvature diagrams for different levels of pressure. It can be observed that as the pressure level increases, the resulting values of maximum curvature $\kappa_{\max}$ decrease for both the UOE and seamless pipes. Fig. 30 and Fig. 31 depict the moment-curvature diagrams for the UOE pipe with ε_{E}=0.66% and a seamless pipe with the same initial ovalization. Both figures show that increasing the level of external pressure both the maximum moment and the maximum curvature decrease. Note that the moment-curvature curves for the seamless pipe are rather smooth due to the plastic plateau of the virgin material in comparison with the more “rounded” curves of the UOE pipe, due to material work-hardening.

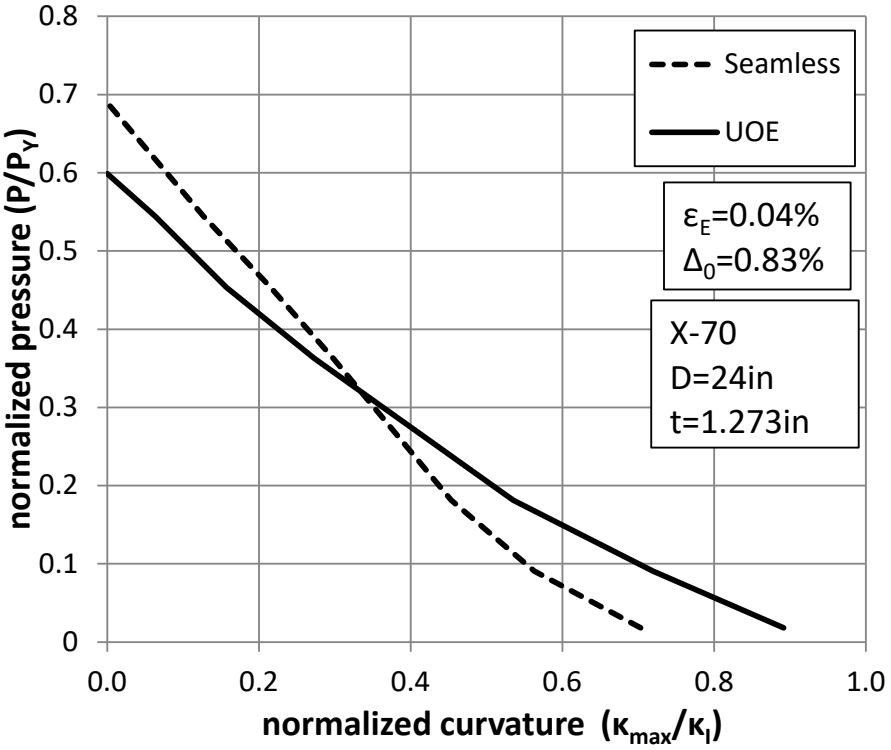

Fig. 24: Pressure-curvature interaction diagram ($P \rightarrow \kappa$) for seamless and UOE pipes for expansion hoop strain ε_E equal to 0.04%.

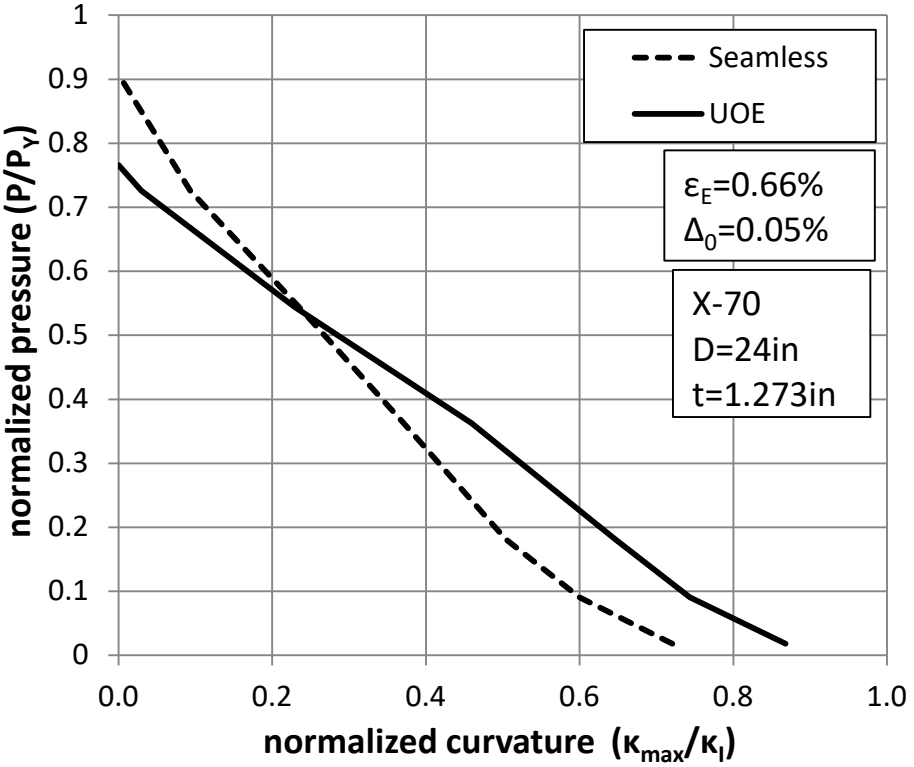

Fig. 25: Pressure-curvature interaction diagram ($P \rightarrow \kappa$) for seamless pipes and UOE pipes for expansion hoop strain ε_E equal to 0.66%.

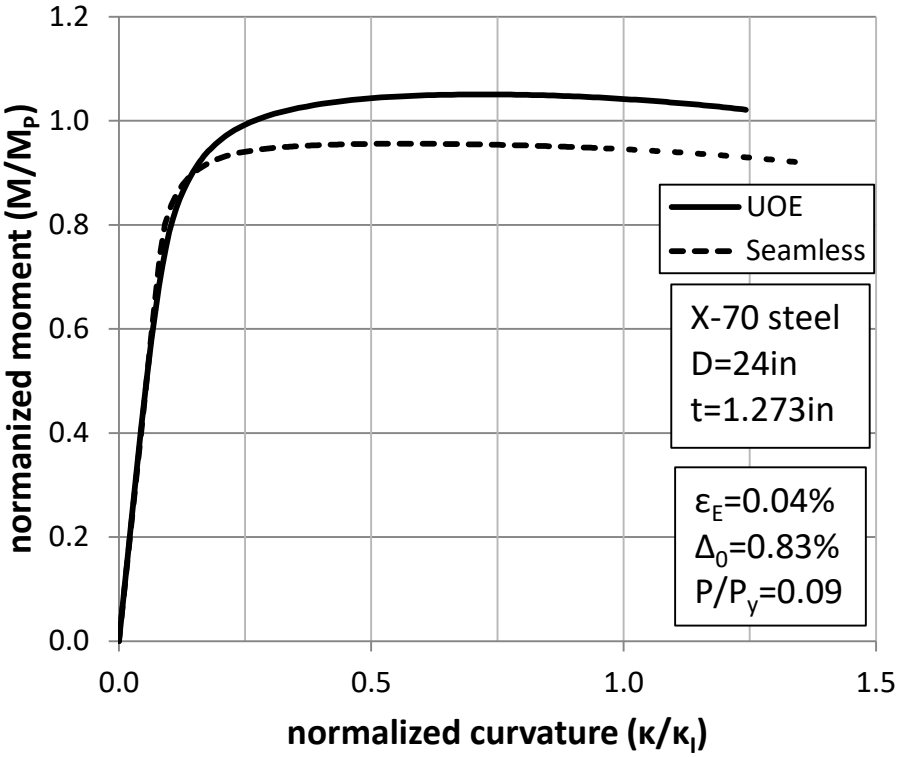

Fig. 26: Moment-curvature diagram in the presence of external pressure, $P / P_y = 0.09$ for expansion hoop strain ε_E equal to 0.04%; comparison with seamless pipe.

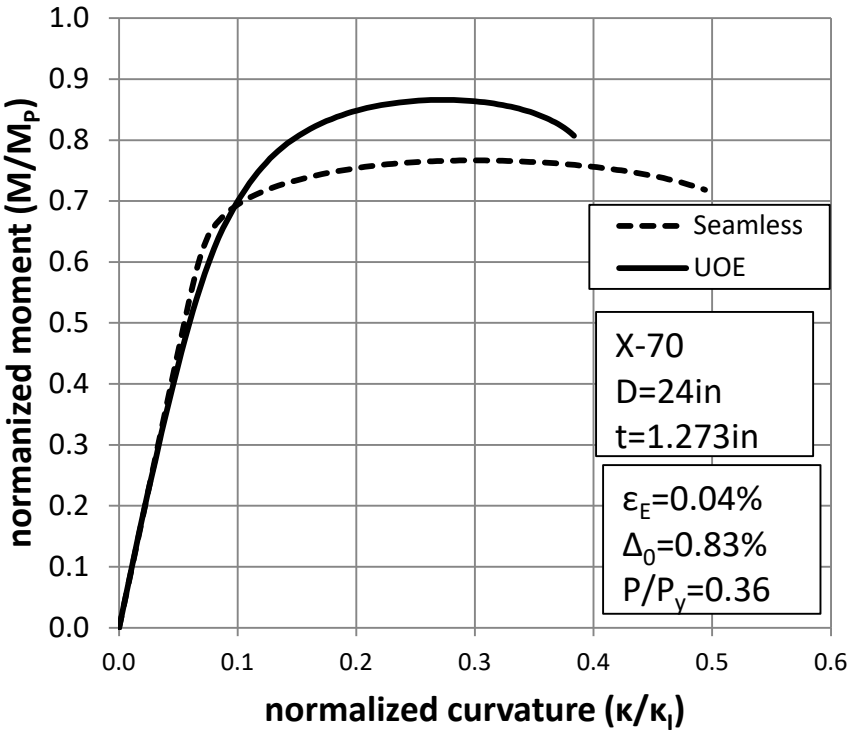

Fig. 27: Moment-curvature diagram in the presence of external pressure, $P / P_y = 0.36$ for expansion hoop strain ε_E equal to 0.04%; comparison with seamless pipe.

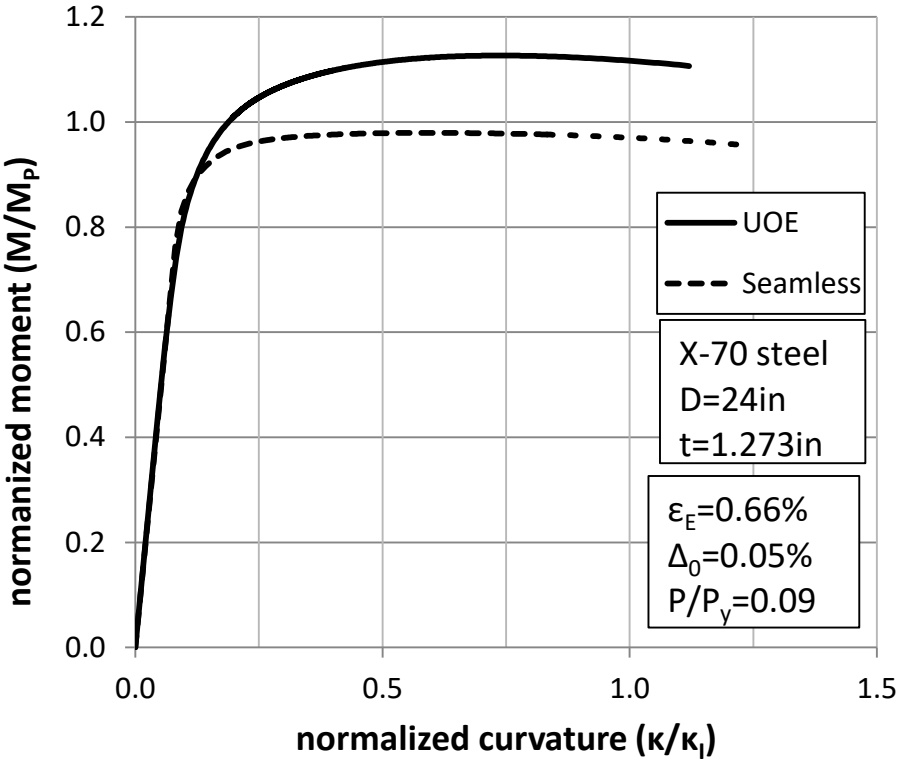

Fig. 28: Moment-curvature diagram in the presence of external pressure, $P / P_y = 0.09$ for expansion hoop strain ε_E equal to 0.66%; comparison with seamless pipe.

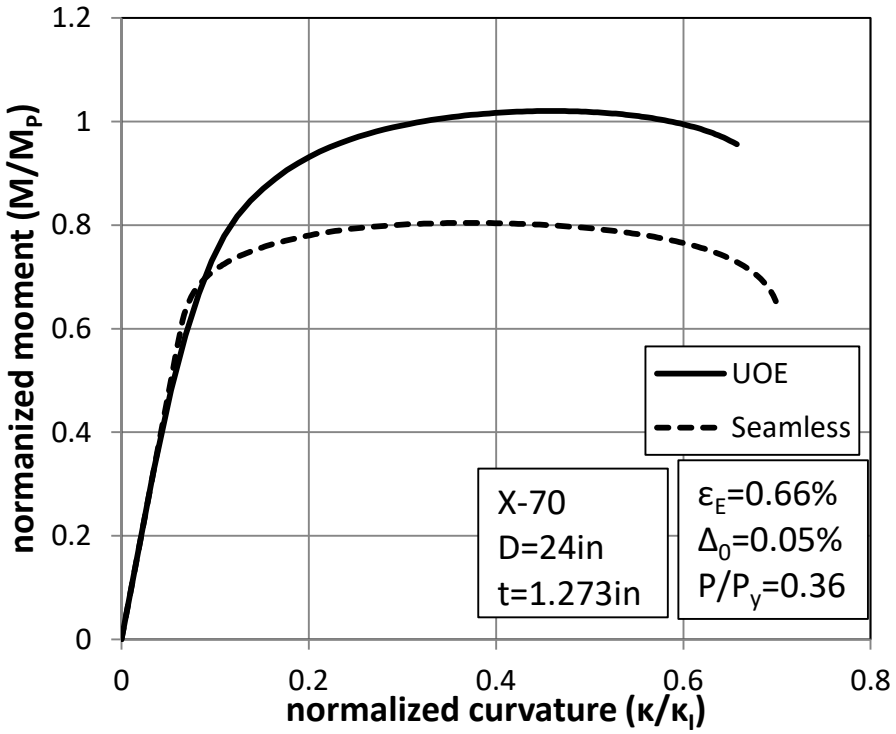

Fig. 29: Moment-curvature diagram in the presence of external pressure, $P / P_y = 0.36$ for expansion hoop strain ε_E equal to 0.66%; comparison with seamless pipe.

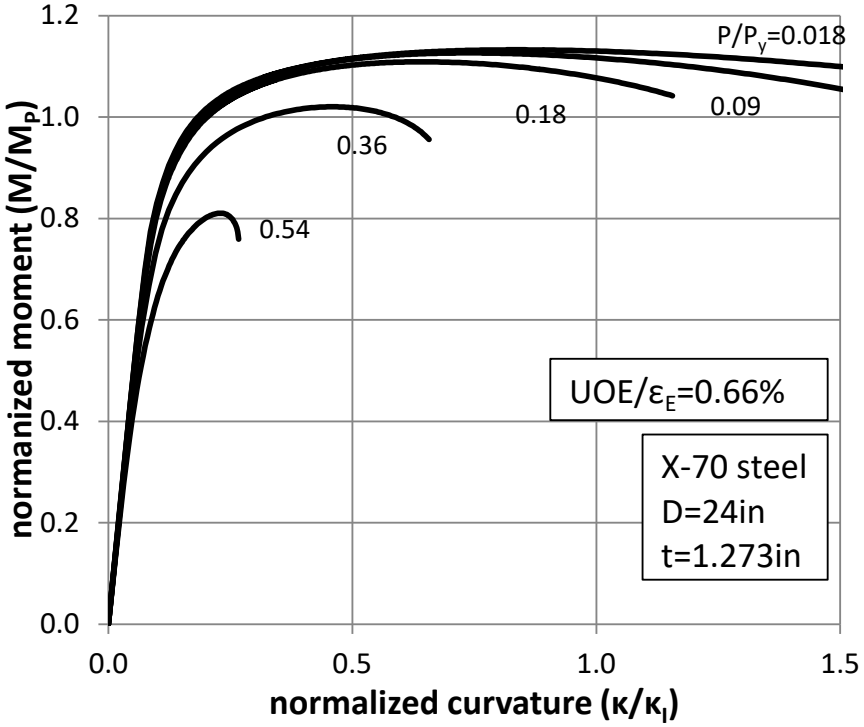

Fig. 30: Moment-curvature diagrams for UOE pipe for different levels of pressure.

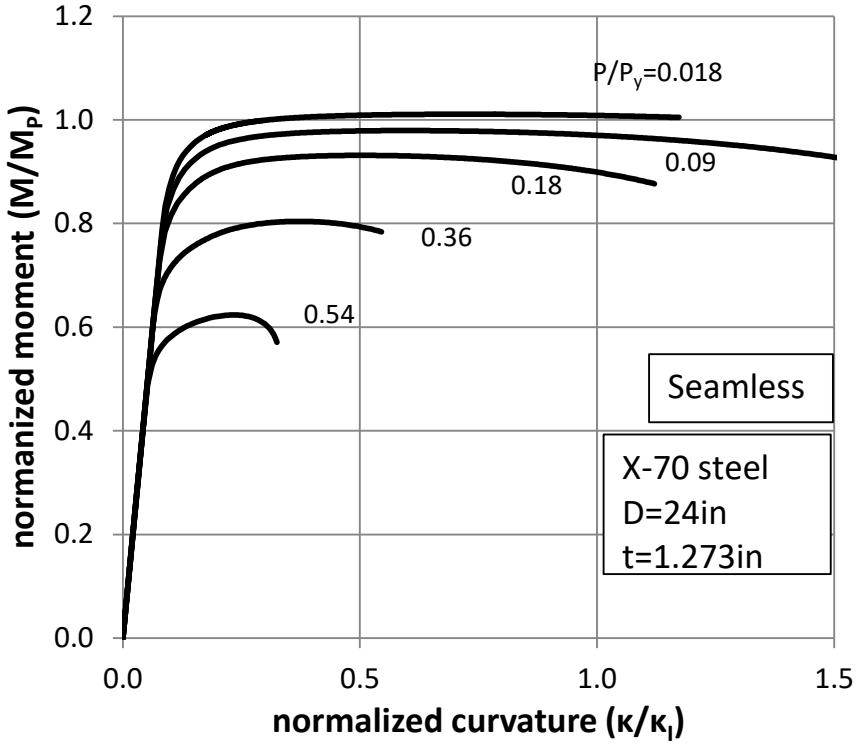

Fig. 31: Moment-curvature diagrams for seamless pipe for different levels of pressure.

5 SIMPLIFIED ANALYSIS FOR PREDICTING THE STRUCTURAL RESPONSE OF UOE PIPES

The effect of UOE line pipe manufacturing process on structural response of thick-walled pipes is also examined using a simplified methodology, which uses more conventional finite element simulation tools. The methodology has been introduced in [3] and is a simple yet efficient method for predicting the ultimate capacity of UOE pipes, as an alternative to the rigorous finite element simulation methodology described in sections 3, 3 and 4. One should notice that the rigorous model requires both knowledge of information for the plate properties and the forming parameters, which may not be available, and advanced skills develop the necessary models and to perform the corresponding simulations of the cold forming process. Furthermore, it is necessary to employ an advanced constitutive model capable of simulating accurately the material behavior under reverse plastic loading conditions.

The extent for material anisotropy induced by the manufacturing process is a key parameter for determining the state of stress, prior to application of pressure and structural loading in a UOE pipe. For the UOE pipes examined in the present study, the anisotropy parameter *S* was found to range from 0.98 to 0.90 according to Fig. 15. In the present paragraph two cases are examined; one case with anisotropy equal to 0.968 corresponding to ε_{E} equal to 0.27% and one case with 0.924 corresponding to $\varepsilon_{\mathrm{E}} = 0.66\%$.

The simplified methodology considers a standard finite element model of the pipe with diameter and thickness equal to the nominal values of the pipe (24 in and 1.273 in respectively) under generalized plane strain conditions. To account for material anisotropy, Hill's anisotropic yield function is considered consistent with anisotropy indicated by the material stress-strain curves shown in Fig. 13. Furthermore, standard isotropic hardening is considered. The above features can be easily found as "built-in" options in several commercial general-purpose finite element programs.

Fig. 32 to Fig. 35 compare the interaction diagrams for the $\mathrm{P} \to \kappa$ and $\mathrm{T} \to \mathrm{P}$ loading sequences, obtained from the above simplified method and from the rigorous model described in the previous sections. The comparison illustrates that the simplified model can provide reliable estimate for the ultimate capacity of the UOE pipe. Therefore, it is concluded that the proposed simplified analysis can be adopted for an efficient analysis of the mechanical behavior of UOE pipes.

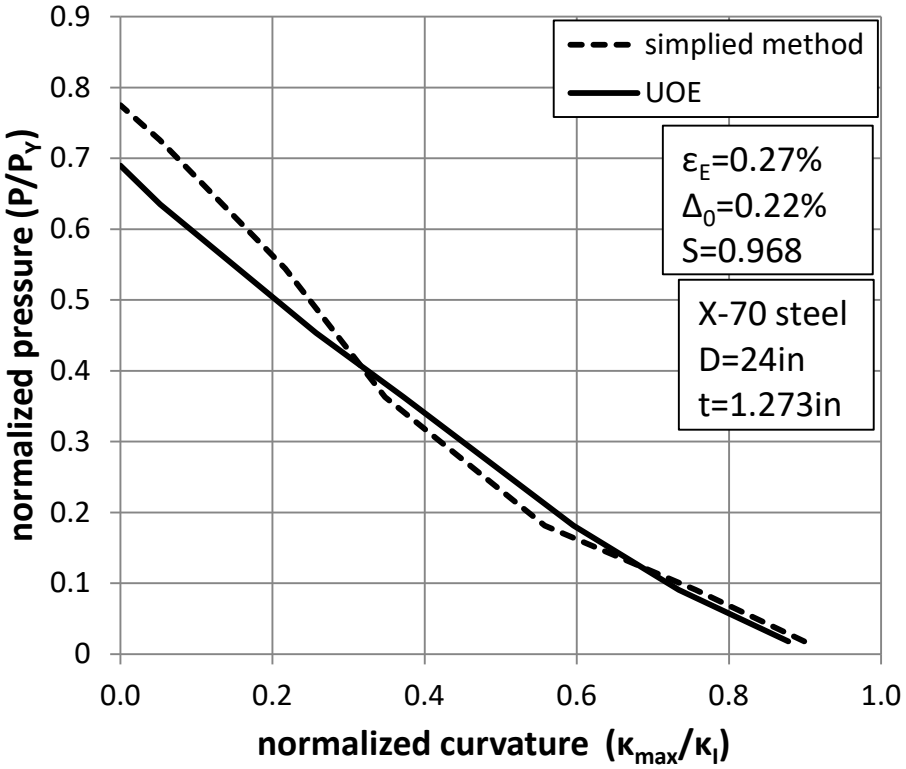

Fig. 32: Pressure-curvature interaction diagram ($P \to \kappa$); comparison of rigorous simulation with the simplified methodology for a UOE pipe with $\varepsilon_E = 0.27\%$.

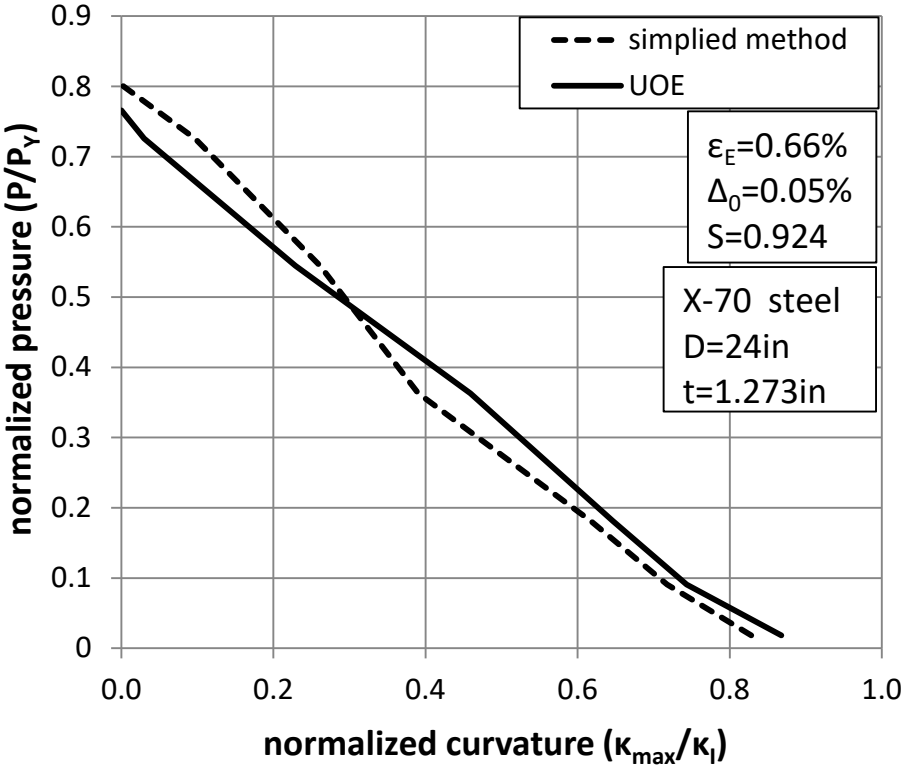

Fig. 33: Pressure-curvature interaction diagram ($P \to \kappa$); comparison of rigorous simulation with the simplified methodology for a UOE pipe with $\varepsilon_E = 0.66\%$.

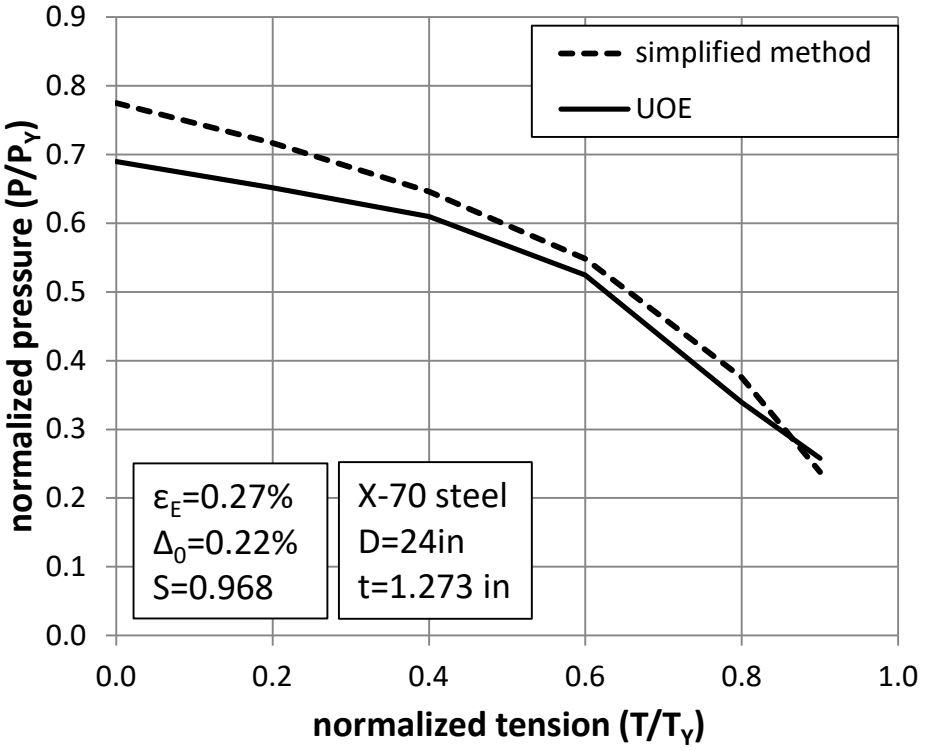

Fig. 34: Tension-pressure interaction diagram ($T \rightarrow P$), Comparison of UOE simulation with the simplified method for UOE pipe with expansion hoop strain ε_E equal to 0.27%.

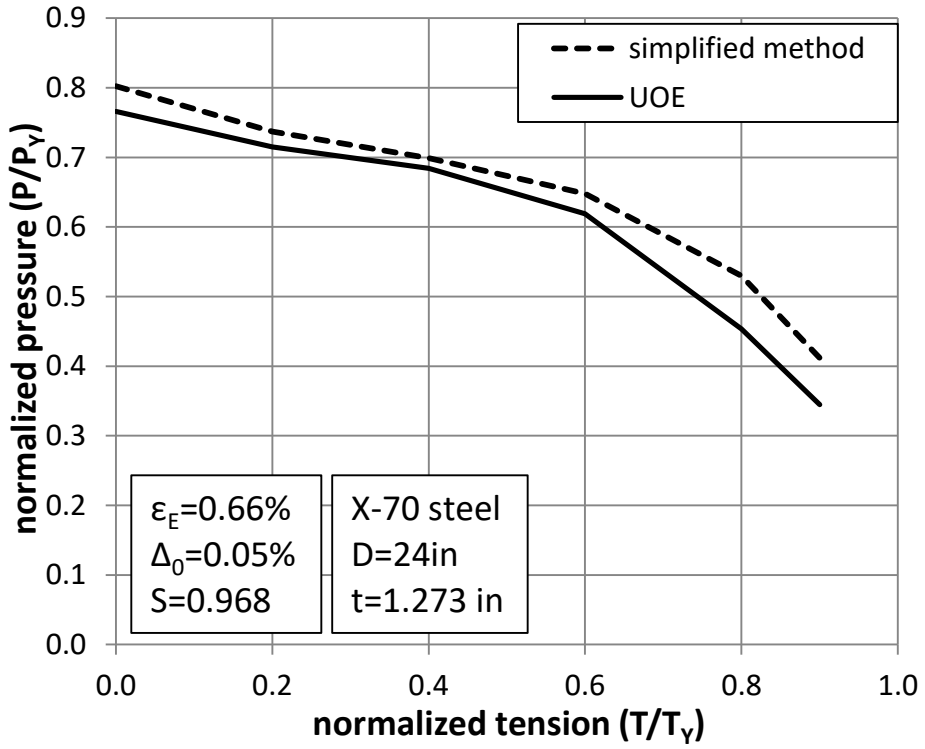

Fig. 35: Tension-pressure interaction diagram ($T \rightarrow P$), Comparison of UOE simulation to simplified method for UOE pipe with expansion hoop strain ε_E equal to 0.66%.

6 CONCLUSIONS

The UOE manufacturing process and its effect on the mechanical behavior of offshore pipes has been studied using advanced finite element simulation tools. An advanced plasticity model, capable of describing the nonlinear elastic–plastic material behavior, is adopted and implemented within the finite element model using a material user subroutine. In the first part of the paper, the UOE cold-bending manufacturing process steps are simulated in detail. The analysis is based on a 24-inch (609.6 mm) diameter pipe with nominal thickness equal to 32.33 mm (1.273 in) and adopts the forming geometrical parameters of a case study introduced elsewhere. A parametric analysis is conducted focusing on the effects of UOE manufacturing process, and in particular those of the expansion stage on the overall pipe behavior against pressure, axial and bending loading. Comparison of the analyzed UOE pipe with the corresponding seamless pipe is also conducted. The numerical results show that the increase of the expansion hoop strain value leads to minimization of pipe out-of-roundness, but beyond a certain expansion value, the collapse pressure resistance of the pipe is reduced due to the Bauschinger effect. As a result, there exists an optimum expansion at which the highest resistance in pressure loading is achieved. Furthermore, the analysis shows that the presence of tension generally decreases the collapse pressure for both UOE and seamless pipes. It is also shown that UOE pipes have lower pressure capacity than seamless pipes for low tension levels, but higher capacity for higher tension levels. This result can be attributed to the strain-hardening effect induced by the forming process. For combined pressure-bending loading conditions, and for relatively low external pressure levels, UOE pipes exhibit higher bending deformation capacity compared to seamless pipes. On the contrary, as the pressure level increases, UOE pipes have less deformation capacity than seamless pipes under bending loading conditions. Finally, a simplified method adopting more conventional finite element simulation tools is described, accounting for the material anisotropy of UOE pipes in the circumferential and axial direction, capable of predicting the ultimate capacity of the pipe within a good level of accuracy and can be used for pipeline design purposes.

REFERENCES

[1] Murphey, C. E., and Langner, C. G., 1985. "Ultimate Pipe Strength under Bending, Collapse and Fatigue", *Proceedings of the 4th International Conference on Offshore Mechanics and Arctic Engineering*, Dallas, USA.

[2] Kyriakides, S., and Yeh, M. K., 1985. "Factors Affecting Pipe Collapse", *Final report to American Gas Association*, Project PR-106-404. Also, University of Texas at Austin, Engineering Mechanics Research Laboratory Report No. 85/1.

[3] Kyriakides, S., and Corona, E., 2007. *Mechanics of offshore pipelines*, Buckling and Collapse, Vol. 1, Elsevier.

[4] Karamanos, S. A., and Tassoulas, J. L., 1995. "Tension Effects on the Pressure Capacity of Tubular Members", *Journal of Structural Engineering*, Vol. 121, pp.955-963.

[5] Corona, E., and Kyriakides, S., 1988. "On the Collapse of Inelastic Tubes Under Combined Bending and Pressure", *International Journal of Solids Structures*, Vol. 24, pp. 505–535.

[6] Karamanos, S. A., and Tassoulas, J. L., 1991. "Stability of Inelastic Tubes Under External Pressure and Bending ", *Journal of Engineering Mechanics*, vol. 117, pp. 2845-2861.

[7] Ju, G. T, and Kyriakides S., 1991. "Bifurcation Buckling Versus Limit Load Instabilities of Elastic-Plastic Tubes Under Bending and External Pressure", *Journal of Offshore Mechanics and Arctic Engineering*, Vol. 113, pp. 43-52.

[8] Kyriakides, S., Corona, E., Fischer, F. J., 1991. "On the Effect of the UOE Manufacturing Process on the Collapse Pressure of Long Tubes", *Offshore Technology Conference* Vol. 4, OTC 6758, pp. 531–543. Also, published in *Journal Engineering for Industry*, Vol. 116, pp. 93–100.

[9] Stark, P. R., and McKeehan, D. S., 1995. "Hydrostatic Collapse Research in support of the Oman-India Gas Pipeline", *Offshore Technology Conference*, Houston, Texas.

[10] Gresnigt, A. M., Van Foeken, R. J., and Chen, S., 2000. "Collapse of UOE Manufactured Steel Pipes", *Proceedings of the Tenth International Offshore and Polar Engineering Conference*, Vol. 2. pp. 170-181, Seattle, Washington.

[11] Gresnigt, A. M., and Van Foeken, R. J., 2001. "Local Buckling of UOE and Seamless Steel Pipes", *Proceedings of the Eleventh International Offshore and Polar Engineering Conference*, pp.131-142, Stavanger, Norway.

[12] Fryer, M., Tait, P., Kyriakides, S., Timms, C., and DeGeer, D., 2004. "The Prediction & Enhancement of UOE-DSAW Collapse Resistance for Deepwater Linepipe", *Proceedings of International Pipeline Conference*, IPC 2004-607, Calgary, Alberta, Canada.

[13] DeGeer, D., Marewski, U., Hillenbrand, H.-G., Weber, B., and Crawford, M., 2004. "Collapse Testing of Thermally Treated Line Pipe for Ultra-Deep Water Applications", *4th International Conference on Pipeline Technology*, Ostend, Belgium.

[14] DeGeer, D., Timms, C., and Lobanov, V., 2005. "Blue Stream Collapse Test Program", *24th International Conference on Offshore Mechanics and Arctic Engineering*, OMAE2005-67260, Halkidiki, Greece, pp. 499-507.

[15] DeGeer D., Timms C., Wolodko J., Yarmuch M., Preston R., MacKinnon D., 2007. “Local Buckling Assessments for the Medgaz Pipeline”, *26th International Conference on Offshore Mechanics and Arctic Engineering*, OMAE2007-29493, San Diego, California, USA.

[16] Herynk, M.D., Kyriakides, S., Onoufriou, A., and Yun, H. D., 2007. "Effects of the UOE/UOC Pipe Manufacturing Processes on Pipe Collapse Pressure", *International Journal of Mechanical Sciences*, Vol. 49, pp. 533–553.

[17] Toscano, R. G., Raffo, J., Fritz, M., Silva, R. C., Hines, J., and Timms, C., 2008. "Modelling the UOE Pipe Manufacturing Process", *Proceedings of 27th International Conference on Offshore Mechanics and Arctic Engineering*, OMAE2008-57605, Estoril, Portugal.

[18] Varelis, G. E., Vathi, M., Houliara, S., and Karamanos, S. A., 2009. "Effect of UOE Manufacturing Process on Pressure Buckling of Thick-Walled Pipes", *X International Conference on Computational Plasticity*, CIMNE, Barcelona.

[19] Tsuru, E., Agata, J., 2013. "Forming and Buckling Simulation on High-strength UOE Pipe with Plastic Anisotropy", *Nippon Steel Technical Report*.

[20] Armstrong, P.J., and Frederick, C.O., 1966. "A mathematical representation of the multiaxial Bauschinger effect", *CEGB Report No. RD/B/N 731*.

[21] Ucak, A., and Tsopelas, P., 2011. "Constitutive Model for Cyclic Response of Structural Steels with Yield Plateau ", *Journal of Structural Engineering*, Vol. 137, No. 2, pp. 195-206.

[22] Chatzopoulou, G., 2014. "Finite Element Simulation of UOE Pipe Manufacturing Process and its Effect on Offshore Pipeline Mechanical Behavior", *Graduate Diploma Thesis, Department of Mechanical Engineering*, University of Thessaly, Volos, Greece.

APPENDIX. DESCRIPTION AND IMPLEMENTATION OF THE CONSTITUTIVE MODEL

Model formulation

The constitutive material model is an extension of the one proposed in [20] for cyclic plasticity. It considers von Mises yield surface, expressed as follows:

$$F = \frac{1}{2}(\mathbf{s}-\mathbf{a})\cdot(\mathbf{s}-\mathbf{a}) - \frac{k^2}{3} = 0 \tag{6}$$

where $\mathbf{s}$ is the deviatoric stress tensor, $\mathbf{a}$ is the back stress tensor and the size of the yield surface $k = k(\varepsilon_q)$ is a function of the equivalent plastic strain ε_q:

$$k(\varepsilon_q) = \sigma_Y + Q(1-e^{-b\varepsilon_q}) \tag{7}$$

In the above expression, σ_Y is the initial value of uniaxial yield stress, Q, b are hardening parameters, and ε_q is the time integral of $\dot{\varepsilon}_q$.

$$\dot{\varepsilon}_q = \sqrt{\frac{2}{3}\dot{\boldsymbol{\varepsilon}}^P \cdot \dot{\boldsymbol{\varepsilon}}^P} \tag{8}$$

The kinematic hardening rule for the back stress tensor rate is adopted

$$\dot{\mathbf{a}} = C\dot{\boldsymbol{\varepsilon}}^p - \gamma \mathbf{a}\dot{\varepsilon}_q \tag{9}$$

where $\dot{\boldsymbol{\varepsilon}}^p$ is the plastic strain rate tensor, and C, γ are parameters calibrated from cyclic test data. In the present formulation to account for the smooth transition from elastic to plastic response, as indicated by the Bauschinger effect, $C = C(\varepsilon'_q)$ is assumed function of equivalent plastic strain ε'_q accumulated at each plastic loading step, as follows:

$$C(\varepsilon'_q) = C_0 + Q_b(1-e^{-c\varepsilon'_q}) \tag{10}$$

where C_0 is the initial value of C at reaching yield surface, whereas Q_b and c are hardening parameters. Finally, the flow rule is given by equation (11)

$$\dot{\boldsymbol{\varepsilon}}^p = \frac{3}{2k(\varepsilon_q)} \dot{\varepsilon}_q (\mathbf{s} - \mathbf{a}) \tag{11}$$

and the rate of stress is related to the rate of elastic strain as follows

$$\dot{\boldsymbol{\sigma}} = \mathbf{D} \, (\dot{\boldsymbol{\varepsilon}} - \dot{\boldsymbol{\varepsilon}}^P) \tag{12}$$

where $\mathbf{D}$ is the fourth-order elastic rigidity tensor.

To represent more accurately structural steel response under monotonic and reverse-plastic loading conditions, an amendment of the constitutive model is necessary to describe both the abrupt change of slope in the stress-strain curve after the initial yielding (yield plateau) and the Bauschinger effect (Fig. 3). This modification follows the proposal of Ucak and Tsopelas [21], defining a critical strain level as the point where the plastic plateau region ends, referred to as the equivalent plastic strain limit, denoted as ε_{ql}. If the computed equivalent plastic strain is less than the value of ε_{ql}, a very small value of the hardening parameter C is assumed, corresponding to plastic plateau. When the critical value ε_{ql} is exceeded or when reverse plastic loading occurs, C becomes the function of the equivalent plastic strain ε'_q expressed by equation (10), representing strain hardening.

Numerical implementation of constitutive model

The numerical implementation of the above model follows an Euler-backward "elastic predictor – plastic corrector" scheme. Given the state parameters $(\mathbf{s}_n, \mathbf{a}_n, \varepsilon_{qn})$ at state *n* and for a given strain increment $\Delta\boldsymbol{\varepsilon}$, the new state parameters at *n*+1 $(\mathbf{s}_{n+1}, \mathbf{a}_{n+1}, \varepsilon_{qn+1})$ are calculated as described below. More specifically, integration of (12) and (11) results in

$$\boldsymbol{\sigma}_{n+1} = \boldsymbol{\sigma}^{(e)} - 2G\Delta\boldsymbol{\varepsilon}^p \tag{13}$$

$$\Delta\boldsymbol{\varepsilon}^p = \frac{3}{2k(\varepsilon_{qn+1})} \Delta\varepsilon_q (\mathbf{s}_{n+1} - \mathbf{a}_{n+1}), \tag{14}$$

where $\Delta(\cdot)$ is the increment of $(\cdot)$ from state *n* to state *n*+1, $\boldsymbol{\sigma}^{(e)} = \boldsymbol{\sigma}_n + \mathbf{D}\Delta\boldsymbol{\varepsilon}$ is the elastic trial stress, and $\Delta\varepsilon_q$ is obtained integrating (8):

$$\Delta\boldsymbol{\varepsilon}_q = \sqrt{\frac{2}{3}\Delta\boldsymbol{\varepsilon}^p \cdot \Delta\boldsymbol{\varepsilon}^p} \tag{15}$$

Furthermore, integration of the back-stress evolution equation (9) results in

$$\mathbf{a}_{n+1} = \mathbf{a}_n + C(\varepsilon'_{q+1})\Delta\boldsymbol{\varepsilon}^p - \gamma\mathbf{a}_{n+1}\Delta\varepsilon_q \tag{16}$$

Enforcing the consistency condition at the final state n+1, and using equations (7), (13), (14), and (16) one results in the following equation in terms of $\Delta\varepsilon_q$

$$\frac{1}{B^2}\left(\mathbf{s}^{(e)} - \frac{1}{1+\gamma\Delta\varepsilon_q}\mathbf{a}_n\right)\cdot\left(\mathbf{s}^{(e)} - \frac{1}{1+\gamma\Delta\varepsilon_q}\mathbf{a}_n\right) - \frac{2}{3}k^2(\varepsilon_{qn+1}) = 0 \tag{17}$$

where

$$B = 1 + \frac{3}{k(\varepsilon_{qn+1})}\left(G + \frac{C(\varepsilon'_{q+1})}{2(1+\gamma\Delta\varepsilon_q)}\right)\Delta\varepsilon_q \tag{18}$$

and $\mathbf{s}^{(e)}$ is the deviatoric part of trial stress $\boldsymbol{\sigma}^{(e)}$. Equation (17) is solved through an iterative Newton–Raphson scheme. Details on the constitutive model and its numerical implementation are offered in [21].